

Article type : Original Manuscript

Palaeo-environment in an ancient low-latitude, arid lacustrine basin with loessite: The Smith Bank Formation (Early Triassic) in the Central North Sea, UK Continental Shelf

*ANNE D. WILKINS**, *ANDREW HURST**, *M.J. WILSON†§* and *STUART ARCHER*‡*

**Department of Geology & Petroleum Geology, University Aberdeen, King's College, Aberdeen AB24 3UE, UK*

†James Hutton Institute, Countesswells Road, Aberdeen, AB15 8QH, UK

§Tomsk Polytechnic University, Tomsk, Russia

‡Dana Petroleum, King's Close, 62 Huntly Street, Aberdeen, AB10 1RS, UK

Corresponding author mail id: a.d.wilkins@abdn.ac.uk

Associate Editor – Nick Lancaster

Short Title – Early Triassic lacustrine basin with loessite

Keywords – Aeolian, arid, Early Triassic, lacustrine, loessite, palaeoclimate, siltstone, wind-blown

This is an Accepted Article that has been peer-reviewed and approved for publication in the *Sedimentology*, but has yet to undergo copy-editing and proof correction. Please cite this article as an “Accepted Article”; doi: 10.1111/sed.12382

This article is protected by copyright. All rights reserved.

ABSTRACT

Predominantly fine-grained strata were deposited in the Smith Bank Formation (Early Triassic) in the Central North Sea area of the Northern Permian Basin. Previously regarded as monotonous red claystone, examination of continuous core reveals abundant stratification, significant variation in colour, siltstone as the prevalent average grain size, and claystone is rare. Loessite occurs beyond the north-western lacustrine margin and aerosol dust has inundated clay pellets derived from aeolian reworking of the desiccated lake floor. The loessite has limited evidence of pluvial reworking but rare fossil roots testify to sufficient moisture to sustain plants. Loessite has not previously been successfully differentiated from other fine-grained strata in the subsurface but this study defines the presence of random grain-fabric orientation as an intrinsic unequivocal characteristic of loessite that formed during air-fall deposition of aerosol dust. Comparison with outcrop data verifies the utility of grain fabric to differentiate loessite. Tosudite, an aluminous di-octahedral regularly ordered mixed-layer chlorite/smectite, which is rare in sedimentary rock, forms a significant proportion (10 to 21%) of the clay mineral fraction of loessite along with a similar quantity of kaolinite. In all other samples, only illite and chlorite are identified, which is typical of fine-grained Triassic strata. In a location, close to the southern lake margin, lacustrine strata are characterised by fining-upward couplets of very-fine grained sandstone into siltstone and mudstone, with occasional desiccated surfaces. Small sand injections and associated sand extrusions are common and indicate periodic fluidisation of sand. Precise stratigraphic location of the Smith Bank Formation is problematic because of extremely sparse fossil preservation however there is no sedimentological evidence for a period of hyper-aridity known from the early Olenekian in continental Europe, which may mean that the North Permian Basin was never hyper-arid or that the Smith Bank Formation is restricted to the Induan.

INTRODUCTION

During the early Triassic in the area of the present-day Central North Sea, an area of major subsidence formed the endorheic Northern Permian basin (Glennie *et al.*,

This article is protected by copyright. All rights reserved.

2003), in which the Smith Bank Formation was deposited. Ephemeral lacustrine environments prevailed (Johnson *et al.*, 1994) where sometimes >1 km of Smith Bank Formation deposited (Stewart, 2007). Sedimentation rate was very slow, the likely maximum rate in the range from 0.14 to 0.27 mm yr⁻¹, that contributed to the pervasive oxidation and reddening of sediment and removed most evidence of fauna and flora. Consequently, the virtually biostratigraphically-barren strata in the Smith Bank Formation are variously described as “*a monotonous sequence of brick-red ... claystones*” (Deegan & Scull, 1977), “*typically monotonous*” (Lervik *et al.*, 1989), “*the monotonous sequences of red... claystones of Scythian age*” (Cameron, 1993) and “*monotonous basal Triassic*” (Goldsmith *et al.*, 2003). Although claystone is the commonly-assigned lithology, none of the previous Smith Bank Formation documentation provides grain-size or mineralogical data to substantiate this interpretation. Similarly, except for the detailed study of the Permo–Triassic strata in onshore and offshore Britain that includes the Smith Bank Formation (Jeans, 2006), there is a paucity of published data pertaining to its palaeo-environment, sedimentology and mineralogy (Wilkins, 2016).

Preliminary observation of core from the Smith Bank Formation reveal that siltstone is common and that lamina-scale lithological and textural heterogeneity are far more apparent than the previously inferred monotony (Deegan & Scull, 1977; Lervik *et al.*, 1989; Cameron, 1993; Goldsmith *et al.*, 2003). Divergent interpretations on similar data clearly require attention both in terms of developing a robust interpretation of the palaeo-environment. If siltstone is a dominant lithology the provenance of large volumes of silt-sized grains requires consideration and aerosol dust deposits may be inferred (Muhs, 2007) if they can be identified in the rock record (loessite; Johnson, 1989). If clay-sized particles and clay minerals are pervasive a provenance associated with chemical weathering of source terrain is requisite (Dixon & Weed, 1989).

The present research aims to question both the monotony and lithological interpretation of ‘claystones’ and thereby investigate the current palaeo-environmental interpretation of the Smith Bank Formation. While recognising the

prevalence of lacustrine conditions this study seeks to provide evidence of changes in lake-level and in general assess the evidence for fluctuations in moisture at and near Earth's surface. Sedimentological evidence for aeolian processes is evaluated in the light of contrasting regional palaeo-environmental interpretations that infer a predominantly lacustrine environment (Goldsmith et al., 2003) and a transition from playa lake (Induan) to playa lakes and aeolian dunes (early Olenkinian) (Bourquin et al., 2010). An important part of the sedimentological analysis includes granulometric analysis of fine-grained strata to constrain depositional processes and the efficacy of granulometric data when differentiating the depositional context of fine-grained strata in core samples or from outcrop. Specific attention is given to identification of loessite, which is previously unrecognised in the Smith Bank Formation and in the subsurface in general, but was considered to be a likely lithofacies in the Permo–Triassic basins of north-west Europe when first described from similar-aged outcrop in North America (Johnson, 1989).

Loessite, 'lithified loess' (Johnson, 1989), is rarely recognised in the geological record and has not been unequivocally differentiated from other fine-grained strata in the subsurface. The lack of unequivocal characteristics that differentiate loessite make it challenging to identify in outcrops but, according to Johnson (1989) can be done based on: (i) the homogeneity and the dominance of the (average) silt grain-size; (ii) the relative lack of primary sedimentary structures; (iii) the gentle character of most bedding contacts and the common mantling of irregular depositional topography; (iv) the inferred palaeogeographic setting; and (v) the absence of suitable alternative interpretations. Using these criteria, several loessites are identified (Soreghan, 1992; Chan, 1999; Soreghan *et al.*, 2002; Soreghan *et al.*, 2007; Evans & Reed, 2007), with few substantive modifications to the list of characteristics from Johnson (1989) required. When examining borehole data the present authors became aware of the limitations of the outcrop characteristics used to identify loessite at outcrop and the need to define unequivocal characteristics in subsurface studies and, more generically, from small samples.

In common with much Quaternary loess, loessite is interpreted to be related to aerosol transport of fine-grained sediment (dust) (Muhs, 2007). Traditionally aerosol

dust that formed loess was interpreted to be derived from high latitude ($>50^\circ$) areas associated with glacial generation of silt-sized material (Pye, 1987). Most present-day aerosol dust is however, derived from the deflation of low-latitude (20 to 40°), low-relief often formerly lacustrine areas undergoing desiccation (Nettleton & Chadwick, 1996; Mahowald *et al.*, 2003). Earth's current most prolific dust source is the combined area of Lake Chad and the Bodélé Depression in sub-Saharan Africa, which produces $>0.77 \text{ Tg day}^{-1}$ in winter and *ca* 60 Tg yr^{-1} (Koren *et al.*, 2006).

Granulometric analysis of loessite derived from petrographic sections provides internally-consistent grain-size distribution analyses that determine loessite to be silt to very-fine sand grade (Johnson, 1989; Chan, 1999; Evans & Reed, 2007). Grain sorting has received little attention (the exception being Evans & Reed, 2007) although the quartz-silt fraction of some loessite is termed well-sorted (Soreghan *et al.*, 2007). No previous analysis of grain fabric orientation is known. Petrographically loessite is known to have quartzo-feldspathic mineralogy (Johnson, 1999; Chan, 1999; Soreghan *et al.*, 2007) and derivation of detritus from source terrain dominated by physical weathering is inferred, indicative of aridity and/or high altitude with low chemical indices of alteration (*cf.* Nesbit & Young, 1982). Separation of zircon, a resistate mineral largely of granitoid origin, from loessite for U/Pb geochronology yields a wealth of provenance data and is used to derive palaeo-wind circulation patterns (Soreghan *et al.*, 2002; 2014). Some loessite has significant concentrations of clay/silt pellets and some evidence of minor amounts of evaporitic minerals (Chan, 1999; Evans & Reed, 2007). Despite the presence of pellets the clay mineralogy of loessite has previously not received detailed attention.

GEOLOGICAL SETTING

Triassic climate has been considered as a simple 'hothouse' world, with ice-free poles and without major climate oscillations (Spalletti *et al.*, 2003). However, two climatically-driven mass extinctions bound the Triassic that are linked to the formation and separation of the Pangaea supercontinent (Kidder & Worsley, 2004; Tanner *et al.*, 2004). The end-Permian mass extinction defines the lower boundary

and coincided with a global increase in temperature of 6 to 8°C (Royer *et al.*, 2004) and predominantly hostile continental climates. This is independently confirmed by general circulation models that conclude that 'global warming' occurred at the Permian–Triassic boundary (Kiehl & Shields, 2005). Extinction of 90% of oceanic species and 70% of vertebrate land life is probable (Erwin, 1994). The early Triassic records a slow recovery of biodiversity that suggests that the harsh conditions that occurred toward the end of the Permian continued to persist for some time (Dickins, 1993; Meyer *et al.*, 2011). The Smith Bank Formation is a record of the early Triassic recovery that is typified by poor preservation of a very sparse fossil record (Goldsmith *et al.*, 2003).

Reconstruction of palaeolatitude using palaeomagnetic data shows that during the early Triassic the Northern and Southern Permian basins lay between 15°N and 25°N of the equator (Westphal *et al.*, 1986; Dinarés-Turell *et al.*, 2005; Hounslow and Muttoni, 2010). This corresponds to a subtropical climate zone (Roscher *et al.*, 2011; Benton & Newell, 2013) that given the continent-ocean configuration (Fig. 1A), the palaeo-European landmass is predicted to have been subjected to pervasive aridity from an imposed subtropical trade wind system that acted as the dominant air-mass circulation system (Feist-Burkhardt *et al.*, 2008). Aeolian deposits preserved in Provence, Sardinia, Cheshire and the East Midlands (Hounslow & Ruffell, 2006) add sedimentological support to the arid climate interpretation (Retallack *et al.*, 1996). The Smith Bank Formation is insufficiently fossiliferous to permit biostratigraphic correlation (Goldsmith *et al.*, 1995) and the absence of interbeds of volcanic ash or lava preclude radiometric dating. Therefore, based only on lithostratigraphic juxtaposition, the Smith Bank Formation is assigned to Induan and Olenekian (equivalent to Scythian) chronostratigraphic stages (Fig. 2) and spans the time period from $247.1 \pm 0.2\text{Ma}$ to $252.2 \pm 0.5\text{Ma}$ (Gradstein & Ogg, 2012). Dealing with up to *ca* 5.8 Ma of unconstrained time combined with sparse availability of continuous core compromises palaeo-environmental interpretation.

In the Southern North Sea, a conformable transition at the base of the Triassic is widely observed in core (Geiger & Hopping, 1968; Geluk, 2005). Similar data are

rare or absent in the Central North Sea where from seismic and borehole (uncored) data the Smith Bank Formation is typically encountered lying directly on Upper Permian strata, most commonly Zechstein evaporites (Goldsmith *et al.*, 2003). Skagerrak Formation or younger strata may overlie the Smith Bank Formation but preservation of this relationship depends upon the extent of the mid-Cimmerian and base Cretaceous unconformities. In areas outside the depositional limits of the Zechstein evaporites where the regional mid-Cimmerian unconformity controls the remaining preserved thicknesses, less than a few hundred metres of Smith Bank Formation is typically encountered (Goldsmith *et al.*, 2003). No post-Zechstein development of extensive evaporites occurred in the North Permian Basin during the Triassic (Bourquin *et al.*, 2011; McKie & Shannon, 2011).

MATERIALS

The study area (ca 35,000 km²) is situated in the UK Central North Sea, specifically the area covered by Quads 20, 21, 22, 23, 29 and 30 (Fig. 1B). Continuous core from >1250 hydrocarbon exploration wells are unsurprisingly biased toward sandstone intervals and only 3% of the released wells have core from Triassic fine-grained strata. Of the 38 wells that cored Triassic mudstone, 31 sample the Smith Bank Formation, and seven sample the Skagerrak Formation. Based on the quality and continuity of available core, wells 20/25-1 and 30/24-22 were selected for detailed study of the Smith Bank Formation, which included sampling for petrographic and mineralogical analysis. The wells are approximately 200 km apart, representing the most north westerly and south easterly parts of the study area (Fig. 1B).

METHODS

Thin section preparation: 40 mm x 25 mm x 15 mm blocks were cut from core samples minimising the use of water to avoid sample degradation. Most blocks were cut perpendicular to depositional laminae when present, with some samples cut parallel to lamination for use in grain fabric determination. To ensure that small-scale sedimentary features would be visible, slides were cut to 20 µm thick and double-polished following the procedure of MacQuaker & Gawthorpe (1993). Double polishing allows slides to be used subsequently for scanning electron microscopy and electron microprobe analysis.

Grain size analysis: Although there are various methods of grain-size analysis available (McManus, 1988), physical sample disintegration followed by sieving then sedimentation by hydrometer, or laser granulometry, was rejected because disintegration would destroy the texture of the samples. Whereas new automated scanning electron microscopy, combined with advanced digital image analysis, can provide detailed textural information at the micro-scale to nano-scale (Camp et al., 2016), the costs associated with such a method were prohibitive. Therefore, the traditional method of grain-size analysis by thin section microscopy was utilised in this study: where limitations include the restricted coverage of sample area, and the limited area of analysis due to high magnification.

Previous thin section studies on grain size analysis of rock samples suggests that up to 500 grain-size measurements are required for a statistically significant measurement (Krumbein, 1935; Greenman, 1951; Friedman, 1958; Kellerhals et al., 1975). The actual number being dependent upon the sorting of the samples, and for a poorly sorted sample around 270 measurements are required for estimation of mean grain size to within 0.1Φ , with a 90% certainty (Johnson, 1994). As such, quantitative petrographic data were acquired from all thin sections with a minimum of 300 counts per slide to maximise confidence while minimising the time expended. When thin sections contained more than one grain-size domain (different lithologies) a separate 300-point count was undertaken in each domain. Each grain-size measurement was made on a scaled, gridded photomicrograph with a calibrated rule and recorded in mm. Measurements were re-scaled and converted to microns (μm) and cumulative frequency curves were plotted along with histograms where the values in mm were converted to the phi (Φ) scale.

While microscopic reporting of grain-size distribution is often used as a semi-quantitative technique, the measurement of the diameter of a three-dimensional grain observed in a two-dimensional planar section does not accurately represent the 3D nature of the grain and is a recognised limitation of this method. It is not the intention here to give a detailed comparison of the various correction factors and methods that can be applied to grain-size determinations. Several theoretical and

empirical methods exist to better estimate a 3D grain-size distribution from 2D measurements: Krumbein (1935), Greenman (1951), Friedman, (1958), Sahu (1966), Packham (1955), Kellerhals et al. (1975), Adams (1977), Harrell & Eriksson (1979), Sahagian & Proussevitch (1998), Kong et al. (2005) and Hinds et al. (2014). In this study a rapid approximation of the true nominal diameter of a measured grain is made by adding 0.05 to the corresponding Φ value (Johnson, 1994); this was undertaken as a correction to the final calculated Φ values.

The sand–silt boundary, which is the distinction between coarse-grained and fine-grained sediment, is placed at 1/16 mm (*ca* 63 μm or +4 Φ), and the sand–pebble boundary is placed at 4 mm or -2 Φ . The upper size limit for clay is 2 μm , a definition in common use in sedimentology (Konert & Vandenberghe, 1997; Blott & Pye, 2012), and in clay mineralogy and soil science (Fernández-Ugalde *et al.*, 2013). Using these definitions sand-silt–clay ternary plots were created with the clay-size fraction defined as <2 μm . Visual comparators were used to estimate grain sphericity, roundness and sorting.

Fabric analysis: For each thin section a fabric domain is defined as an area that is statistically homogenous on the scale of the domain. Fabric domains are typically delineated by natural surfaces such as sedimentary laminae. A fabric is treated as an ordered array of discontinuities, and the aim of fabric analysis is to establish this order and represent it in graphic form.

Using photomicrographs each non-equant grain, whose minimum width to length ratio was 1:3, was highlighted within specific domains. Each grain was numbered and its angle of departure from a horizontal reference datum recorded. A minimum of 50 measurements were taken for each photomicrograph. Equal-area rose diagram circular plots were used to display the orientation of the grains measured, where the data count is tallied for 10° bins. A planar fabric is recorded when grains are observed not to be randomly orientated within a specific fabric domain. A random fabric is defined when domains lack distinct preferred orientation.

This article is protected by copyright. All rights reserved.

As for grain-size analysis, fabric analysis by thin section microscopy has similar method limitations that include the finite coverage of sample area, and the restricted area of analysis due to high magnification.

Scanning Electron Microscope (SEM) and Energy Dispersive Spectroscopy (EDS): Carbon-coated double-polished thin sections were analysed using an ISI-ABT55 electron microscope (Akashi Beam Technology Corporation, Tokyo, Japan) to determine textural relationships and energy-dispersive spectra to aid identification of individual minerals.

X-Ray Diffraction (XRD) – sample preparation and analysis: Special care was taken when sampling core to avoid the outer margins so as to minimise any potential contamination by drilling mud. In most instances a *ca* 20g subsample block was cut from the core at the same time as the thin section subsample, but where limited material remained, representative cuttings and trimmings from the thin section block were used. Thereafter procedures followed those of Hillier (1999) for preparation of X-ray random powder diffraction (XRPD). The XRD patterns were obtained either from a Siemens D5000 (Siemens, Munich, Germany) with a θ/θ goniometer, using Co K α radiation, a diffracted-beam monochromator with 1^o slits and counting for 1s per 0.02^o 2 θ step through the range 2^o 2 θ to 75^o 2 θ , or from a Philips Xpert (PANalytical, Almelo, The Netherlands) with a θ/θ goniometer, using Cu radiation, a diffracted beam monochromator with 1^o slits and counting for 0.4s per 0.02^o 2 θ step through the range 3^o 2 θ to 45^o 2 θ . Quantitative analysis of the bulk sample patterns was performed using a full pattern fitting and a computational reference intensity ratio (Hillier, 2003). Values of weight fractions (X) are given with a level of confidence of 95% and an estimate of expanded uncertainty of $\pm X^{0.35}$.

Clay fractions (<2 μ m) were derived from suspensions of washed (in deionised water), ultrasonically-dispersed samples that were left for 16 hours, after which the suspension was syphoned off to a depth of 10cm within a cylindrical flask thus removing the <2 μ m fraction. Smooth, flat, homogeneous clay mounts were obtained

following the millipore filter transfer method (Drever, 1973). Clay samples were run either from $3^{\circ}2\theta$ to $45^{\circ}2\theta$ on a Philips Xpert with a θ/θ goniometer, using Cu K α radiation, a diffracted beam monochromator, 1° slits and counting for 0.4s per $0.02^{\circ}2\theta$ step, or, from $2^{\circ}2\theta$ to $75^{\circ}2\theta$ on a Siemens D5000 with a θ/θ goniometer, using Co K α radiation, a diffracted-beam monochromator with 1° slits and counting for 1s per $0.02^{\circ}2\theta$ step. Clay mineral identification of the $<2\ \mu\text{m}$ fractions was determined by observing the responses of the diagnostic basal reflections following air drying, treatment with ethylene glycol, heating at 300°C and treatment with 6N HCl at 95°C for 30 minutes.

RESULTS

Core observations

Well 20/25-1 is dominated by largely unstratified siltstone with a paucity of sedimentary structures that accounts for approximately 80% of the core (*ca* 11 m) (Fig. 3A); the unstratified siltstone is a candidate loessite. Bed thickness varies from approximately 0.6 to 1.4 m. Most of the siltstone is micro-micaceous with flakes of muscovite and biotite a few hundred microns across and visible to the naked eye. The siltstone is generally red-orange brown in colour (Fig. 4A) with some notable grey or green-grey reduction mottling or bleaching (Fig. 4B). Occasional burrows and rhizomes are present, as are 15 mm and 30 mm thick, erosive-based, thin beds and laminae of stratified siltstone or trough cross-laminated, very-fine grained sandstone (Fig. 4C). Stratified very-fine grained sandstone, siltstone and claystone constitute the remaining 20% of the core and occur at the base and top of the cored section.

By contrast, well 30/24-22 consists entirely of stratified claystone, siltstone and very fine sandstone (Fig. 3B). Unstratified siltstone is rare and thin beds of very fine-grained sandstone are common. The thin beds and laminae of very fine-grained sandstone, siltstone and claystone are typically laterally continuous across the width of the core, and display sub-millimetre to millimetre scale ($<1\ \text{mm}$ to $15\ \text{mm}$) lamination that includes horizontal parallel, parallel curvilinear, ripple and trough cross-lamination (Fig. 5A). Very fine-grained sandstone forms pale grey-red or grey,

usually sharp-based beds up to 25 mm thick, occasionally with scoured bases with intra-formational lags of claystone clasts. Siltstone and claystone are red-brown to dark red except where localised reduction occurs and forms green-grey and grey areas, respectively. Stratification is thin, usually <20 mm, and horizontal parallel lamination occurs at approximately 100 µm spacing where, because of the colour variations, at least 15 laminae per 10 mm interval are discernible. Downward-tapering sediment-filled shrinkage cracks are constrained to specific claystone horizons and caused by desiccation (Fig. 5B). Probable pedogenic slickensides are identified in one location. Sediment injection is pervasive, predominantly as centimetre to decimetre-length (height) siltstone to very fine sandstone dykes (Fig. 5C). Sandstone, siltstone and mudstone are prevalent throughout the central cored section, between 9820' and 9835' but mudstone is notably less common towards the top of the section where there is a higher proportion of sandstone.

Petrographic observations

Candidate loessite siltstone in well 20/25-1 comprises varying proportions of angular quartz and feldspar, muscovite and biotite, clay pellets and diagenetic dolomite. Quartz and feldspar grains tend to be silt-sized, whereas the mica is the hydraulically-equivalent fine sand-size (Fig. 6A). Clay pellets are generally rounded to well-rounded (Fig. 6B and C) and are of very fine to fine sand-size to coarse silt-size. A pervasive randomly-oriented fabric defined by mica grains is characteristic (Fig. 7A). Clay pellets have a consistent internal planar fabric (Fig. 7B) that contrasts with the random fabric within the unstratified siltstone host. Dolomite is entirely diagenetic and irregular pore-filling dolomite is the predominant cement. Dolomite also occurs as euhedral rhombs scattered throughout the groundmass and as pseudomorphs of halite (Fig. 6D). Dolomite crystals are zoned but inclusion-rich cores are uncommon. Occasional red-brown hematite-stained, anhedral cores are present in several morphological forms. In sample SB10 (5455.5' MD) dolomite accounts for nearly one third of the mineralogy and is almost exclusively pore-filling and zoned, with inclusion-rich cores and less included, clearer rims. No more than three concentric zones of varying clarity are observed.

During EDS analysis particles of baddeleyite (ZrO_2) were identified. This is a rare mineral (Lumpkin, 1999) never before identified in sedimentary rock (Wilkins et al., 2015). Grains were only ca 4 μm across and thus undetectable in thin section. However, because of its high density (5.75 g cm^{-3}) and simple composition, baddeleyite is readily differentiated by EDS.

Stratification is pervasive in well 30/24-22 where siltstone and claystone laminae prevail and vary from hundreds of microns to as little as 30 μm thick (Fig. 8A). The thinnest laminae are characterised by single-grain layers (Fig. 8B) that are sometimes discontinuous (Fig. 8C). Sub-horizontal and sub-vertical burrows, ca 100 to 300 μm wide and with a quartz-rich, coarse silt-sized fill and clay-rich surrounds, occur in some siltstone units.

Textural evaluation

Grain size distribution: Quantitative petrographic grain-size analysis shows that siltstone is the predominant lithology present in both wells. In well 20/25-1, which is the candidate loessite, the average grain size distribution is 6.3% sand-sized, 67.8% silt-sized and 25.9% clay-sized particles (Fig. 9). Four samples (SB03, SB05, SB06 and SB08) are from unstratified siltstone with non-erosive bases and with grain size predominantly in the range of 4Φ to 5Φ , with a mean grain diameter of between 5.29Φ and 6.02Φ . The grain-size distributions of the samples are generally bi-modal, negatively skewed and very poorly sorted (Fig. 10). Exceptions to this are mudstone laminae, which have significantly different grain size domains within stratified siltstone sample SB10, that on average contain 10% more clay-sized grains and thus plot within the mudstone field (Fig. 9). The unstratified siltstone has randomly-orientated grain fabrics consisting chiefly of predominantly angular quartz grains.

A more restricted range of grain size characteristics are present in well 20/25-1 (Fig. 10A to C) than in well 30/24-22 (Fig. 10D to H). Within sample EQ02, very fine sandstone laminae are significantly more enriched in sand-sized particles (up to

21.7%). Also, the only genuine claystone is encountered within sample EQ04 (grain-size domain EQ04a, Fig. 10D) in which claystone laminae occur that consist of 98% clay-sized particles. On average, samples from well 30/24-22 contain 50% clay-size material, which is approximately double the amount encountered in the average sample from well 20/25-1. Grain size data from both wells do not support the earlier contentions that the Smith Bank Formation consists of monotonous claystone (Deegan & Scull, 1977; Lervik et al., 1989; Cameron, 1993; Goldsmith et al., 2003).

Grain shape and sorting: Both unstratified and stratified strata contain predominantly angular to sub-angular, predominantly quartz, silt and coarser grains of varying sphericity (Fig. 11A and B). Minor amounts of rounded to well-rounded grains occur but these are almost exclusively in the >50 μm coarse silt to very fine sand size-range, the coarsest fraction present. Clay pellets, which are common in the unstratified siltstone (Fig. 6B and C) are ellipsoidal in section and well-rounded, although broken pellets have at least one angular margin. A <2 μm to 150 μm grain-size range, indicative of poor to very-poor sorting, is present in all samples (Fig. 11C and D). In general, siltstones from well 20/25-1 are slightly better-sorted and the same samples have a smaller range of grain size distributions (Fig. 11C) than samples from well 30/24-22 (Fig. 11D). Grain-size distribution curves are concave-upward for coarser siltstone, for example sample EQ02b, and convex-upward as the finer grained content increases, for example sample EQ06.

Grain fabric determination: Random, planar and bi-modal grain fabrics are identified. Random grain fabric occurs within the unstratified siltstone (candidate loessite) of well 20/25-1 and is typified by an equal weighting of elongate detrital grains in all orientations and a lack of clear preferred orientation (Fig. 12A). Planar fabric displays a prominent preferred orientation (Fig. 12B and C) and is most commonly encountered within the finely-laminated siltstone and claystone of well 30/24-22, where elongate minerals lie approximately $\pm 10^\circ$ either side of horizontal. Planar fabric is also observed in the stratified siltstone and mudstone in well 20/25-1. In both wells ripple laminated, very-fine sandstone and coarse siltstone have planar fabrics that are inclined most commonly between 20° to 30° and 150° to 160° from

horizontal. Bi-modal fabrics occur in claystone with shrinkage cracks (Fig.12D); the sub-horizontal population reflects the primary planar fabric, while the sub-vertical population represents the orientation of the cracks. The greater the proportion of sub-vertical orientations, the greater the apparent influence of shrinkage on the primary planar fabric. The interplay between the two populations produces the bi-modal distribution. Bioturbation disturbs primary planar fabrics thus producing a more random grain fabric (Fig.12E) but without the equal proportions of all orientations present in the unstratified siltstone (Fig. 12A).

Bulk Mineralogy

Well 20/25-1. Quartz content varies from 35.6 to 46.9%, feldspar content is quite high with albite averaging 6.8% (ranging from 5.4 to 7.5%) and alkali feldspar (K-feldspar) averaging 6.5% (ranging from 5.2 to 6.5%) (Fig. 13A). Orthoclase is usually the dominant K-feldspar, with microcline subordinate, and sanidine present in trace amounts. Calcite was not identified in any of the samples but dolomite is pervasive, varying in abundance between 1.8% and 11.8% and, exceptionally, reaching 29.5% in a stratified mudstone (sample SB10). Hematite averages *ca* 2% in red coloured samples, but is present only in trace amounts in samples with greenish grey colouration, e.g. SB06 and SB10. Halite is ubiquitous but uncommon (<1.5%).

Illite, chlorite and kaolinite are present in all samples. Tosudite is present in all samples except samples SB08 and SB10. Trace amounts of expandable mixed-layer illite/smectite are present. The clay minerals were first identified in the <2 μm (clay-size) fraction, then quantified in the bulk (XRPD) samples. On average the total percentage of clay minerals in the bulk rock is 35%, but varies from as little as 23% within the stratified mudstone SB10, to as much as 41% within the unstratified siltstone SB05; thus, clay mineral content does not correspond to the abundance of the clay-size particle fraction. Illite predominates in the XRPD analyses but some of that volume is likely to be detrital mica that has the same d-spacing as illite and is known from thin section petrography. The full pattern fit of the XRPD trace does not

differentiate between illite and muscovite. Similarly, detrital chlorite may account for part of the chlorite identified by XRPD.

Well 30/24-22. Quartz content varies from 21 to 28% except for a bioturbated siltstone (sample EQ05), which contains 37% quartz (Fig. 13B). Plagioclase (albite) content averages 6.3% (ranging from 4.6 to 8.3%) but alkali feldspar averages 3.6% (ranging from 2.9 to 4.9%), approximately half the abundance seen in well 20/25-1. However, the ratios of these three framework silicate minerals are similar in both wells, where 20/25-1 and 30/24-22 have average ratios of 76:13:11 and 73:17:10, respectively. Dolomite is significantly more abundant in most samples from well 30/24-22 compared to well 20/25-1, varying between 26.2% and 31.3%. The exception to this is sample EQ05 (bioturbated siltstone) that contains only 0.9% dolomite. Hematite is only detected in pervasively red samples, where up to 2.4% is present (sample EQ05). Halite is found in all samples in trace amounts only (<0.1%). Illite is the dominant clay mineral present (23.1 to 38.2%) and occurs together with chlorite. Kaolinite and tosudite were not detected.

Clay Mineralogy of the <2 μm fraction

Relative proportions of clay minerals in the bulk samples and the clay fraction are distinctly different in terms of their mica/illite (non-expandable 10Å basal spacing) content. Proportionately, there is significantly more mica/illite in the bulk samples than in the clay fractions, which indicates the presence of significant amounts of mica/illite in the silt-size and sand-size fractions. This reflects the micro-micaceous nature of the Smith Bank Formation samples as a whole, and is confirmed by thin section observations and back-scattered SEM images where many mica flakes are observed, some being up to 150 μm in length, both in the matrix and in clay pellets. The 'illite' in the clay-size fraction may be fundamentally different to the 'mica' observed in the bulk samples because it responds to ethylene glycol treatment as is shown below.

Well 20/25-1. The clay mineral suite comprises illite, mixed-layer illite–smectite (I/S), chlorite, kaolinite and tosudite (a di-octahedral regularly ordered, mixed-layer chlorite–smectite). Quantitative results reveal that the clay fractions are dominated by illitic minerals (illite + I/S) with a mean content of 55.9% and ranging from 45 to 66%. Kaolinite, chlorite and tosudite have mean contents of 16.1% (ranging from 9 to 23%), 14.0% (ranging from 13 to 18%) and 13% (ranging from 10 to 21%), respectively. Chlorite, illite and kaolinite were identified by their diagnostic basal reflections, which for chlorite occur at 14.1, 7.05, 4.72 and 3.54Å, for illite at 10.0, 5.0 and 3.35Å, and for kaolinite at 7.14 and 3.57Å (Fig. 14A and B). Mixed-layer I/S showed a clear response to ethylene glycol treatment in that the 10Å peak for illite noticeably sharpened, an effect which is usually interpreted as indicating a small number of interstratified smectite layers (*ca* 5 to 10%) arranged in an ordered structure such that every smectite (S) layer is succeeded or preceded by three illite (I) layers in a sequence such as IIIS; this is usually referred to as an R3 arrangement (Reynolds, 1980). Tosudite was identified by a high spacing, first order basal reflection at *ca* 28Å which expands to *ca* 32Å on glycolation and contracts to *ca* 24Å on heating. Additionally, tosudite is highly aluminous and resists decomposition by HCl treatment, serving to distinguish it from corrensite, which is trioctahedral, magnesium-rich and yields similar basal reflections to tosudite, but decomposes completely in HCl (Fig. 14B; Wilson, 2013).

Well 30/24-22. The clay mineralogy in this well is significantly different from that of well 20/25-1 in that it is dominated by an illite–chlorite assemblage, with no indication of either kaolinite or tosudite (Fig. 14C). It is important to note, however, that the illitic material consists both of illite and mixed-layer I/S. The clay fraction is even more illite-dominated than well 20/25-1 with a mean illite + I/S content of 77% (ranging from 71 to 82%). Mean illite content is 43% (ranging from 38 to 47%), mean I/S content is 35% (ranging from 21 to 41%) and mean chlorite content is 23% (ranging from 18 to 29%). Illite–chlorite assemblages are typical of the Triassic mudstone sequences in the Julius, Jonathan and Joshua mudstone members of the overlying Skagerrak Formation.

Comparative data from loessite in Triassic and Permian formations, Utah

As part of the validation of the unstratified siltstone from well 20/25-1 as loessite, samples were taken from outcrops in Utah of known loessites, to compare their textural and mineralogical characteristics with the Smith Bank Formation: viz the Ankareh (Triassic) and Halgaito (Permian) formations (Murphy, 1987; Chan, 1999). All samples are siltstone, with varying concentrations of silt-sized clay pellets and minor amounts of rounded to well-rounded, almost exclusively, very fine sand grains (Fig. 15A and B); the samples classify as siltstone (Fig. 15C). Grain-size distribution data reveal a range of grain sizes from $<2\ \mu\text{m}$ to $116\ \mu\text{m}$ and are very poorly to poorly sorted (Fig. 16). Grain fabric analysis reveals random orientation similar to that observed in the Smith Bank Formation loessite in well 20/25-1 (Fig. 12A). Rare calcite-filled halite pseudomorphs are observed (Parleys Canyon, sample PC01) as are calcite-filled rootlets (Mexican Hat, sample MH02).

DISCUSSION

Wells 20/25-1 and 30/24-22 have the best preserved continuous core from the Smith Bank Formation, and are located close to the north western and south eastern margins of the lacustrine basin described by Goldsmith et al. (2003). Both of the cored intervals are dominated by siltstone (Fig. 9), but 20/25-1 is sparsely stratified whereas 30/24-22 is pervasively stratified (Fig. 3). Neither core readily corresponds with earlier descriptions of monotonous claystone.

Palaeoenvironment – moisture

In well 20/25-1 the cored interval is dominated by siltstone (Fig. 3A) formed by suspension fall-out of aerosol dust (Johnson, 1989; Soreghan *et al.*, 2007). Loess, the progenitor of loessite, deposits in wet or dry atmospheric conditions, forming a coarse unimodal grain-size distribution when associated with dry deposition and, a distinctive bimodal grain-size distribution when deposited during rainfall (Hesse & McTainsh, 1999). Both bimodal and unimodal grain-size distributions are present in Smith Bank Formation loessite (Fig. 10A to C), thus recording periods of aerosol

dust deposition during periods when atmospheric moisture varied. Random grain fabric is consistent with air-fall deposition and minimal aqueous reworking (Mücher et al., 1981). Pluvial run-off (rainwash, Mücher et al., 1981) is interpreted to have formed the subordinate, poorly-sorted, centimetre-scale fining-upward units of very fine to fine-grained sandstone inter-laminated with finer-grained strata. Long periods without significant rainfall (enough to produce pluvial flow) are inferred.

Clay pellet formation is compatible with aeolian processes during progressive lacustrine desiccation, typically leeward of dust sources (Price, 1963; Bowler, 1973), and is consistent with the persistent lacustrine palaeo-environment inferred for the Smith Bank Formation (Goldsmith et al., 2003; Bourquin et al., 2010; Fig. 17A). In the loessite, clay pellets are largely silt to very fine sand grade and form among the largest particles present, and are anomalously-rounded relative to the angular, finer-grained quartzo-feldspathic groundmass (Fig. 6A and B). Pellets form when desiccation causes the decomposition of formerly-submerged muddy surfaces and creates mobile aeolian aggregates of sand-sized clay particles. As pellets are blown leeward they gather as clay dunes (often lunettes) on raised areas adjacent to lake shores and become stabilised by hygroscopic moisture absorption and/or vegetation (Price, 1963). Clay pellets in the 20/25-1 loessite are inferred to have been transported by prevailing winds from the south-east (Uličný, 2004) to the north-west area of the lake margin where they became inundated by periodic aerosol dust falls.

Well 30/24-22 has stratified deposits that are consistent with low-energy water-lain deposition in which the coarsest units are current-rippled, very fine sandstone laminae (Fig. 5A). Sand deposition formed predominantly sub-centimetre scale units interpreted to be single unidirectional flow events. Occasional compound centimetre-scale units occur that record periods of more sustained flow. Sandstone laminae have sharp, erosive, occasionally scoured (millimetre-scale) bases and sharp upper surfaces that are draped by mudstone or siltstone. Some primary lamination is disrupted by periods of desiccation during which sand- and silt-filled cracks form (Fig. 5B) and, later and more pervasively by sand fluidisation and injection (Fig. 5C). Sedimentation in well 30/24-22 was entirely lacustrine and estimated to be *ca* 10 km

offshore of the southern lacustrine margin (Fig. 17B). Clastic input into this area of the Central North Sea was minor (Goldsmith et al., 2003; Bourquin et al., 2010; McKie & Shannon, 2011), thus it is unlikely that the sandstone laminae are distal parts of basin-fringing alluvial fans, for which there is no direct evidence, but more likely to be reworked shoreline deposits. Planar grain fabrics are consistent with deposition from unidirectional current flow and have a pervasive linearity (Fig. 12B and C) that when disrupted by desiccation cracks and clastic intrusions produce a bimodal grain fabric (Fig. 12D) and when bioturbated have a random-like grain fabric (Fig. 12E).

Deposition of the Smith Bank Formation occurred during a period of global aridity (Péron et al., 2005; Bourquin et al., 2010); however, in the detail of the rock record of the North Permian Basin there is abundant evidence for the presence and significance of water. Desiccation cracks, which are only locally common, are constrained to claystone horizons that by definition must have previously been water-saturated. Seven periods of desiccation are discernible, implying seven sub-aqueous periods when the substrate was water saturated (Fig. 5B). Direct evidence of major aeolian deposition, reported by Bourquin et al. (2010), is absent as concluded by McKie and Williams (2009). Thin, often discontinuous single-grain-thick coarse-silt laminae (Fig. 8A and B) are the only direct record of aeolian deposition and are interpreted as deposits from low-elevation dust clouds that blew across the lake surface. The present authors assume that these volumetrically tiny deposits are indicative of deflation of the lake shoreline to the south of the well location; this cannot be validated.

More spectacular evidence of moisture is the common occurrence of small-scale siltstone/sandstone intrusions that occasionally preserve less than centimetre-scale thick sand extrusions that formed when sand was fluidised in the very shallow (5 to 20 cm) subsurface (Fig. 5C). When preserved, the extrusions prove that they formed sub-aqueously. The <10 cm high sand injection illustrated, is among the largest observed and, cross-cuts at least twelve depositional couplets of sandstone and mudstone/siltstone. Sand fluidisation implies that a sealing unit, in this case the

laminated sandstone and mudstone/siltstone couplets into which sand was injected, overlay a sandstone layer (the parent unit) into which pore-fluid pressure (P_f) rose too rapidly to bleed off: P_f eventually exceeded the fracture pressure of the seal thus causing hydraulic failure and flow of fluidised sand into the fracture system (Vigorito & Hurst, 2010; Hurst et al., 2011). To enable sand injection to occur the following conditions were probably necessary: (i) a very shallow water table; (ii) a subaqueous surface; (iii) a rapid rise of P_f in the parent unit. Conditions (i) and (ii) imply standing water and a likely regional rise of the water table in the aquifer, and (iii) requires focused subsurface flow toward the interval where hydraulic failure occurred. Focused subsurface flow is likely to accompany a rapid rise in lake level along or near to the lake margin.

Differentiating loessite

All loessite examined is characterised by random grain-fabric orientation (Figs 12A and 15D), a texture that is unequivocally diagnostic. All other granulometric characteristics observed are as expected for loessite (Johnson, 1989), predominantly silt grain-size (Fig. 9), angular to sub-angular grain shape (Figs 6, 7 and 11), bimodal grain-size distribution (Fig. 10) and poor sorting (Fig. 11A) but none of these differentiate loessite from the other fine-grained lithofacies. Grain-size distribution is less widely spread (Fig. 11 A) than in the stratified deposits (Fig. 11B) and marginally better sorted; these differences record that more heterogeneous lithofacies are present in stratified units and record fluctuating depositional conditions. Prevailing poor to very poor sorting and random grain fabric are diagnostically uncharacteristic of the granular homogeneity described by Johnson (1989); indeed all loessite in this study is pervasively heterogeneous with homogeneity possibly only reflecting the average grain size.

Because the random grain-fabric forms during aerosol dust deposition it is an intrinsic characteristic relating directly to the process of formation. This is consistent with grain fabric textures described from loess (Matalucci et al., 1969; Derbyshire et al., 1988) and by visual comparison with loessite studied by others (Johnson, 1989;

Chan, 1999; Soreghan et al., 2007). Sparse internal structures and occasional preservation of rootlets and burrows in 20/25-1 are consistent with outcrop loessite descriptions in which a paucity of internal structures is deemed characteristic (Johnson, 1989; Chan, 1999; Soreghan et al., 2007). Defining loessite as siltstone with sparse internal structures giving an unstratified homogenous appearance, is however inadequate as an unequivocal diagnostic characteristic, because a lack of stratification may have other depositional or post-depositional origins, for example, intense bioturbation. Thus, homogeneity and dominance of the sandy silt grain size, used as diagnostics in the original characterisation of loessite (Johnson, 1989), are in the present study only the first approximations suggestive of loessite. Characteristics used to differentiate outcrop of loessite from other fine-grained deposits, such as lateral continuity and sheet-like geometry (Johnson, 1989), have little relevance to core examination and are not unequivocally diagnostic.

Mineralogy

Apart from the identification of major rock-forming minerals in loessite, there is a paucity of published mineralogical data. All of the samples herein have quartz-rich and illite/muscovite-rich depositional compositions with a subordinate but similar quantity and composition of feldspar (Fig. 13). Preservation (>10%) of feldspar (plagioclase + K-feldspar) and muscovite is high, which is suggestive of derivation of detritus from source terrain dominated by physical weathering, aridity and/or high altitude. This is typical of Palaeozoic and early Mesozoic loessite and associated fine-grained strata (Johnson, 1999; Chan, 1999; Soreghan et al., 2007).

Zircon U/Pb geochronology of loessite contributed significantly to the reconstruction of late Palaeozoic monsoonal atmospheric circulation (Soreghan et al., 2002; 2007; 2014). Because zircon is a resistate heavy mineral largely of granitoid origin, it is useful for determining ages of granite unroofing in orogenic belts however, if other resistate and non-resistate heavy minerals are present they will almost certainly enhance the understanding of loessite provenance, weathering of the source terrain and diagenetic transformations (Morton, 2012; Hurst & Morton, 2014). When heavy

minerals are incorporated into aerosol dust they are finer grained than the average size of the co-existing quartz and feldspar, largely because of density differences. For example, when tourmaline ($\delta = 2.82$ to 3.32 g cm^{-3}) coexists with zircon ($\delta = 4.6$ to 4.7 g cm^{-3}) it tends to be coarser and both are finer grained than co-existing quartz and feldspar (hydraulic equivalence with coarse silt to very fine sand grains requires zircon to be smaller than fine silt-size). The first-ever discrete (ca $4 \mu\text{m}$ diameter) baddeleyite (ZrO_2 , $\delta = 5.5$ to 6.0 g cm^{-3}) in sedimentary rock was made from loessite in well 20/25-1, in a heavy mineral suite that includes zircon, Fe-Ti oxides and ilmenite (Wilkins et al., 2015).

Illite–chlorite clay mineralogy prevails, which is typical of the strata investigated in this study and is widespread in Permo–Triassic of the North Sea as a whole (Jeans, 2006; Ziegler, 2006). Illite–chlorite assemblages are typically associated with burial diagenesis and burial temperatures in the range of >80 to 150°C (Lee et al., 1989; Ziegler, 1993; Hillier et al., 1996). The studied section in well 20/25-1 is currently buried at ca 1650 m and from regional temperature data is unlikely ever to have been heated above 50°C thus suggesting that the illite–chlorite assemblage is detrital. If so, then the illite and chlorite in well 20/25-1, and elsewhere in the Smith Bank Formation, were reworked by erosion of source terrain that previously was heated to temperatures in excess of the range noted above. Such reworking of clay minerals typical of a higher diagenetic grade is not unusual (Hurst, 1982; Hurst, 1985), the lack of alteration of illite and chlorite during erosion and deposition, being a function of dominantly physical weathering.

In the loessite, the occurrence of tosudite and kaolinite in addition to illite and chlorite is remarkable (Fig. 14), but at present its significance is unclear. Most findings of tosudite are associated with hydrothermal activity (Wilson, 2013), but in well 20/25-1 its occurrence is constrained to the loessite lithofacies, in which case a genetic relationship may exist between tosudite and loessite. It is unlikely that tosudite is a diagenetic phase, such as recorded in the British Devonian (Hillier et al, 2006), because well 20/25-1 does not appear to have undergone significant heating ($<50^\circ\text{C}$) during burial. The question of whether clay mineralogy is useful as a

criterion for distinguishing loessite evidently requires further work, in particular an assessment of the relative roles of provenance, diagenesis and aeolian deposition.

Palaeoenvironmental synthesis

During deposition of the Smith Bank Formation a large Early Triassic hinterland existed (probably $>100,000 \text{ km}^2$) that included extensive mountainous areas (Feist-Burkhardt et al., 2008; Bourquin et al., 2010; McKie & Shannon, 2011) from which physical weathering reworked and preserved feldspar, mica, illite and chlorite (Jeans, 2006). Lake level was controlled by precipitation largely derived from a mountainous catchment, whereas evidence of precipitation in the study area is sparse. Loessite contains minimal evidence of pluvial events. Early Olenekian hyper-aridity (Bourquin et al., 2011) is not identified in the Smith Bank Formation. Either hyper-arid conditions did not prevail, or the early Olenekian cannot be differentiated, or is absent in the cored sections. Despite the sparse sedimentological evidence for moisture, the presence of rootlets in the loessite (Fig. 3A) proves that the terrestrial substrate could support vegetation. It may be that extreme aridity is not required to remove most evidence of fossil material during a *ca* 60 kyr period of very-slow sedimentation ($0.14 \text{ to } 0.27 \text{ mm yr}^{-1}$) and pervasive oxidation.

Lacustrine conditions prevailed in the study area (Fig. 17A; Johnson et al., 1994; Goldsmith et al., 2003; McKie & Shannon, 2011), however, in the southern area of the basin well 30/24-22 records long periods (*ca* 88 kyr) in which changes to a shallow regional water table were rapid enough to induce sand fluidisation and extrusion onto a subaqueous lake floor. By contrast periods of low lake-level caused desiccation. Minor clastic input (Fig. 5A and B) is presumably derived from an unconstrained Variscan source to the south (Bourquin et al., 2011). In contrast the north-western margin of the basin (well 20/25-1, Fig. 17B) has no direct evidence of lacustrine sedimentation but rather a record of aerosol dust deposition that contains only minor evidence of pluvial reworking. Clay pellets diagnostic of lacustrine desiccation (Price, 1963; Bowler, 1973) confirm that periodic variations in lake level occurred and that the prevailing wind direction was from the south-east (Uličný,

2004). No evidence is preserved for major clastic input from inferred generally northern sources (McKie & Shannon, 2011).

CONCLUSIONS

During the early Triassic, deposition of the Smith Bank Formation records persistent lacustrine sedimentation during a period of pervasive aridity. Desiccated surfaces evidence periods of lake-level fluctuation, with very minor evidence of evaporite formation. Small-scale sandstone intrusions record rapid rises of lake-level that were probably induced by rapidly-changing water-tables, conditions that are indicative of less aridity than those traditionally associated with the Smith Bank Formation.

Loessite is positively identified for the first time in the Smith Bank Formation, and random grain-fabric orientation is established as an intrinsic unequivocal diagnostic of loessite. This enables the identification of loessite in boreholes, and where outcrops are poorly exposed. Where subaqueous reworking of loessite occurs, the siltstone has a planar grain fabric. Random grain fabric orientation should be routinely applied to identify and differentiate loessite from other fine-grained facies. Loessite records a prolonged period of aerosol dust deposition adjacent to the ancient lake margin and contains clay pellets derived from periods of sustained aeolian reworking of a desiccated lake floor.

Quartz-rich siltstone prevails throughout the Smith Bank Formation in stratified lacustrine strata or as (unstratified) loessite. Evidence for 'monotonous claystone' deposition formerly associated with ephemeral lacustrine deposition is unusual. Despite sparse core availability, sedimentological data compel significant modifications to the palaeo-environmental interpretation and locally constrain the northern and southern margins of lacustrine conditions, loessite in the north and lacustrine facies in the south. No evidence is found for the early Olenekian hyper-arid period recorded further south.

Preservation of muscovite and biotite in an otherwise feldspathic, quartz–siltstone is indicative of physical weathering processes. This is confirmed by the dominance of detrital illite and chlorite in the clay fraction, except in the loessite where tosudite and kaolinite occur. Tosudite is a di-octahedral regularly ordered, mixed-layer chlorite–smectite and is uncommon in sedimentary rock. Although the paragenesis of the tosudite–kaolinite assemblage is not understood, the tosudite is possibly of detrital origin but further work is required to confirm this supposition.

Acknowledgements

This work was conducted as part of the Triassic Mudstones Joint Industry Project which was sponsored by BP, ConocoPhillips, EON E&P, Esso Exploration and Production UK Limited, GDF SUEZ E&P UK Ltd, JX Nippon, Maersk Oil, Shell and Total. The guidance of Prof. Steve Hillier of the James Hutton Institute in quantitative mineralogical analysis is acknowledged with gratitude. Dr Stuart Jones and an anonymous referee are thanked for their incisive and constructive reviews that significantly helped in the revision of the manuscript.

REFERENCES

Adams, J. (1977) Sieve Size Statistics from Grain Measurement. *Journal of Geology*, **85**, 209-227.

Benton, M.J. and Newell, A.J. (2013) Impacts of global warming on Permo-Triassic terrestrial ecosystems, *Gondwana Research*,
<http://dx.doi.org/10.1016/j.gr.2012.12.010>

Blakey, R. (2006) *Mollewide plate tectonic maps – Early to Middle Triassic (240Ma)*
<http://jan.ucc.nau.edu/~rcb7/mollglobe.html>.

Blott, S. J. and Pye, K. (2012) Particle size scales and classification of sediment types based on particle size distributions: Review and recommended procedures. *Sedimentology*, **59**, 2071-2096.

Bourquin, S, Bercovici, A., López-Gómez, J., Diez, J. B., Broutin, J., Ronchi, A., Durand, M., Arché, A., Linol B. and Amour, F. (2011) The Permian–Triassic transition and the onset of Mesozoic sedimentation at the northwestern peri Tethyan domain scale: Palaeogeographic maps and geodynamic implications. *Palaeogeography, Palaeoclimatology, Palaeoecology*, **299**, 265–280.

Bowler, J. M. (1973) Clay dunes: their occurrence, formation and environmental significance. *Earth-Science Reviews*, **9**, 315-338.

Brennard, T. P. (1975) The Triassic of the North Sea. *In: Woodland, A.W. (ed) Petroleum and the Continental Shelf of Northwest Europe*. Applied Science Publishers, London, pp. 295-311.

Cameron, T.D.J. (1993) 4. Triassic, Permian and pre-Permian of the Central and Northern North Sea. *In: Knox, R.W. O'B. & Cordey, W.G. (eds) Lithostratigraphic nomenclature of the UK North Sea*. British Geological Survey, Nottingham.

Camp, W.K., Egenhoff, S., Schieber, J., and Slatt, R.M. (2016) A compositional classification for grain assemblages in fine-grained sediments and sedimentary rocks- discussion. *Journal of Sedimentary Research*, **86**, 1-5.

Chan, M. A. (1999) Triassic loessite of north-central Utah; stratigraphy, petrophysical character, and paleoclimate implications. *Journal of Sedimentary Research*, **69**, 477-485.

Deegan, C.E. and Scull, B.J. (1977) *A standard lithostratigraphic nomenclature for the Central and Northern North Sea*. Institute of Geological Sciences Report 77/25: NPD-Bulletin No. 1.

Derbyshire, E., Billard, A., Vliet-Lanoë, V., Lautridou, J.P., and Cremaschi, M. (1988) Loess and palaeoenvironment: some results of a European joint programme of research. *Journal of Quaternary Science*, **3**, 147-169.

Dickins, J.M. (1993) Climate of the Late Devonian to Triassic. *Palaeogeography, Palaeoclimatology, Palaeoecology*, **100**, 89-94.

Dinarés-Turell, J., Diez, J.B., Rey, D. and Arnal, I. (2005) "Buntsandstein" magnetostratigraphy and biostratigraphic reappraisal from eastern Iberia: Early and Middle Triassic stage boundary definitions through correlation to Tethyan sections. *Palaeogeography, Palaeoclimatology, Palaeoecology*, **229**, 158-177.

Dixon, J.B. and Weed, S.B. (1989) Minerals in Soil Environments, 2nd Edition (Soil Science Society of America Book Series), 1207 pp.

Drever, J.I. (1973) The preparation of orientated clay mineral specimens for X-ray diffraction analysis by the filter-membrane peel technique. *American Mineralogist*, **58**, 553-554.

Erwin, D.H. (1994) The Permo-Triassic extinction. *Nature*, **367**, 231-236.

Evans, J.E. and Reed, J.M. (2007) Integrated loessite-paleokarst depositional system, early Pennsylvanian Molas Formation, Paradox Basin, southwestern Colorado, U.S.A. *Sedimentary Geology*, **195**, 162-181.

Feist-Burkhardt, S., Götz, A. E., Szulc, J., Borkhataria, R., Geluk, M., Haas, J., Hornung, J., Jordan, P., Kempf, O., Michalik, J., Nawrocki, J., Reinhardt, L., Richen, W., Rholing, H.-G., Ruffer, T., Török, Á. and Zühlke, R. (2008) Triassic. In: McCann, T. (ed) *The Geology of Central Europe, Volume 2: Mesozoic and Cenozoic*, The Geological Society, London, pp. 749-822.

Fernández-Ugalde, O., Barré, P., Hubert, F., Virto, I., Girardin, C., Ferrage, E., Caner, L. and Chenu, C. (2013) Clay mineralogy differs qualitatively in aggregate-

size classes: clay-mineral-based evidence for aggregate hierarchy in temperate soils. *European Journal of Soil Science*, **64**, 410–422.

Friedman, G.M. (1958) Determination of sieve-size distribution from thin-section data for sedimentary petrological studies. *Journal of Geology*, **66**, 394-416.

Geiger, M.E. and Hopping, C.A. (1968) Triassic stratigraphy of the Southern North Sea Basin. *Philosophical Transactions of the Royal Society of London*, **B254**, 1-36.

Geluk, M. (2006) *Stratigraphy and tectonics of Permo-Triassic basins in the Netherlands and surrounding areas*. Unpublished PhD thesis. Utrecht University.

Glennie, K.W., Higham, J. and Stemmerik, L. (2003) *In: Evans, D., Graham, C., Armour, A. & Bathurst, P. (eds) The Millennium Atlas: Petroleum Geology of the Central and Northern North Sea*. The Geological Society, London, 91 –103.

Goldsmith, P.J., Hudson, G. and van Veen, P. (2003) Triassic. *In: Evans, D., Graham, C., Armour, A. & Bathurst, P. (eds) The Millennium Atlas: Petroleum Geology of the Central and Northern North Sea*. The Geological Society, London, 105-127.

Goldsmith, P.J., Rich, B. and Standring, J. (1995) Triassic stratigraphy in the South Central Graben, UK North Sea. *In: Boldy, S. A. R. (ed), Permian and Triassic Rifting in Northwest Europe*. The Geological Society, London, Special Publication, **91**, 123–143.

Gradstein, F.M. and Ogg, J.C. (2012) Chapter 2. The chronostratigraphic scale. *In: Gradstein, F. M., Ogg, J. C., Schmitz, M. & Ogg, G. (eds), The Geologic Time Scale*. Elsevier, Oxford, pp. 31-42.

Greenman, N.N. (1951) The mechanical analysis of sediments from thin-section data. *Journal of Geology*, **59**, 447-462.

Harrell, J., and Eriksson, K. (1979) Empirical conversion equations for thin-section and sieve derived size distribution parameters. *Journal of Sedimentary Research*, **49**, 273-280.

Hesse, P.P. and McTainsh, G.H. (1999) Last glacial maximum to early Holocene wind strength in the mid-latitudes of the Southern Hemisphere from aeolian dust in the Tasman Sea. *Quaternary Research*, **52**, 343-349.

Hillier, S. (1999) Use of an air brush to spray dry samples for X-ray powder diffraction. *Clay Minerals*, **34**, 127-135.

Hillier, S., Fallick, A. E, and Matter, A. (1996) Origin of pore-lining chlorite in the Aeolian Rotliegend of northern Germany. *Clay Minerals*, **31**, 153-171.

Hillier, S., (2003) Quantitative analysis of clay and other minerals in sandstones by X-ray powder diffraction (XRPD). *In: Worden, R.H. & Morad, S. (eds) Clay Mineral Cements in Sandstones*. International Association of Sedimentologists, Special Publication, **34**, 213-251.

Hillier, S., Wilson, M.J. and Merriman, R.J. (2006) Clay mineralogy of the Old Red Sandstone and Devonian sedimentary rocks of Wales, Scotland, and England. *Clay Minerals*, **41**, 433-471.

Hinds, O., Duller, R. A., Walker, R. P., Wells, B. T. and Worden, R. H. (2014) Enhanced Two Dimensional Grain Size Analysis through the Use of Calibrated Digital Petrography. *AAPG Search and Discovery*, Article #41461.

Hounslow, M.W. and Ruffell, A. (2006) Triassic - seasonal rivers, dusty deserts and salty lakes. *In: Brenchley, P.J. & Rawson, P.F. (eds), The Geology of England and Wales*, The Geological Society of London, London, 295-324.

Hounslow, M.W. and Muttoni, G. (2010) The geomagnetic polarity timescale for the Triassic: linkage to stage boundary definitions. *In: Lucas, G. (ed), The Triassic Timescale*, Geological Society, London, Special Publication, **334**, 61-102.

This article is protected by copyright. All rights reserved.

Hurst, A. and Morton, A.C. (2014) Provenance models: the role of sandstone mineral–chemical stratigraphy. In: *Sediment Provenance Studies in Hydrocarbon Exploration and Production*, Bath, Geological Society, London, Special Publications **386**, 7-26.

Hurst, A. (1982) The clay mineralogy of Jurassic shales from Brora, NE Scotland. In: Van Olphen H. and Veniale, F. (eds), *International Clay Conference 1981*, Developments in Sedimentology 35, Elsevier, 677-684.

Hurst, A. (1985) The implications of clay mineralogy to palaeoclimate and provenance during the Jurassic in NE Scotland. *Scottish Journal of Geology*, **21**, 143-160.

Hurst, A., Scott, A. and Vigorito, M. (2011) Physical characteristics of sand injectites, *Earth-Science. Reviews*, **106**, 215-246.

Jeans, C. J. (2006). Clay mineralogy of the Permo-Triassic strata of the British Isles: onshore and offshore. *Clay Minerals*, **41**, 309-354.

Johnson, H., Warrington, G. and Stoker, S.J. (1994) 6. Permian and Triassic of the Southern North Sea. In: Knox, R. and Cordey, W.G. (eds) *Lithostratigraphic nomenclature of the UK North Sea*. British Geological Survey, Nottingham.

Johnson, M.R. (1994) Thin section grain size analysis revisited. *Sedimentology*, **41**, 985-999.

Johnson, S.Y. (1989) Significance of loessite in the Maroon Formation (middle Pennsylvanian to lower Permian), Eagle basin, Northwest Colorado. *Journal of Sedimentary Petrology*, **59**, 782-791.

Kellerhals, R., Shaw, J. and Arora, V.K. (1975) On grain size from thin sections. *Journal of Geology*, **83**, 79-96.

Kidder, D.L. and Worsley, T.R. (2004) Causes and consequences of extreme Permo–Triassic warming to globally equable climate and relation to Permo–Triassic extinction and recovery, *Palaeogeography, Palaeoclimatology, Palaeoecology*, **203**, 207–237.

Kiehl, J.T. and Shields, C.A. (2005) Climate simulation of the latest Permian: Implications for mass extinction. *Geology*, **33**, 757-760.

Koren, I., Kaufman, Y.J., Washington, R., Todd, M.C., Rudich, Y., Martins, J.V., and Rosenfeld, D. (2006) The Bodélé depression: a single spot in the Sahara that provides of the mineral dust to the Amazon forest. *Environmental Research Letters*, **1**, 014005 doi:10.1088/1748-9326/1/1/014005.

Konert, M. and Vandenberghe, J. E. F. (1997) Comparison of laser grain size analysis with pipette and sieve analysis: a solution for the underestimation of the clay fraction. *Sedimentology*, **44**, 523-535.

Kong, M., Bhattacharya, R.N., James, C. and Basu, A. (2005), A statistical approach to estimate the 3D size distribution of spheres from 2D size distributions: *Geological Society of America Bulletin*, **117**, 244-249.

Krumbein, W.C. (1934) Size frequency distribution of sediments. *Journal of Sedimentary Petrology*, **4**, 65-77.

Krumbein, W.C. (1935) Thin-section mechanical analysis of indurated sediments. *Journal of Geology*, **43**, 482-496.

Lervik, K.S., Spencer, A.M. and Warrington, G. (1989) Outline of Triassic stratigraphy and structure in the central and northern North Sea. *In*: Collinson, J.D. (ed.) *Correlation in hydrocarbon exploration*. Graham and Trotman, London, 173-189.

Lee, M., Aronson, J.L., and Savin, S.M. (1989) Timing and conditions of Permian Rotliegendes sandstone diagenesis, southern North Sea: K/Ar and oxygen isotope data. *Am. Assoc. Petrol. Geol. Bull.*, **73**, 195-215.

MacQuaker, J.H.S. and Gawthorpe, R.L. (1993) Mudstone lithofacies in the Kimmeridge Clay Formation, Wessex Basin, Southern England: implications for the origin and controls of the distribution of mudstones. *Journal of Sedimentary Petrology*, **63**, 1129-1143.

Mahowald, N., Luo, C., del Corral, J., and Zender, C.S. (2003) Interannual variability in atmospheric mineral aerosols from a 22-year model simulation and observational data. *Journal of Geophysical Research*, **108**, 1-20.

Matalucci, R.V., Shelton, J. W., and Abel-Hardy, M. (1969) Grain orientation in the Vicksburg loess. *Journal of Sedimentary Petrology*, **39**, 969-979.

McKie, T. and Williams, B.P.J. (2009) Triassic palaeogeography and fluvial dispersal across the northwest European Basins. *Geological Journal*, **44**, 711–741.

McKie, T. and Shannon, P.M. (2011) Comment on “The Permian–Triassic transition and the onset of Mesozoic sedimentation at the northwestern peri Tethyan domain scale: Palaeogeographic maps and geodynamic implications” by S. Bourquin, A. Bercovici, J. López-Gómez, J. B. Diez, J. Broutin, A. Ronchi, M. Durand, A. Arché, B. Linol and F. Amour. *Palaeogeography, Palaeoclimatology, Palaeoecology*, **311**, 136–143.

McManus J. (1988) Grain size determination and interpretation. *In: Tucker M (ed.). Techniques in Sedimentology.* Blackwell, Oxford, 63–85.

Meyer, K.M., Yu, M., Jost, A.B., Kelley, B.M. and Payne, J.J. (2011) $\delta^{13}\text{C}$ evidence that high primary productivity delayed recovery from end-Permian mass extinction. *Earth and Planetary Science Letters*, **302**, 378-384.

Morton, A.C. (2012) Value of heavy minerals in sediments and sedimentary rocks for provenance, transport history and stratigraphic correlation. In: Sylvester, P. (ed.), *Quantitative Mineralogy and Microanalysis of Sediments and Sedimentary Rocks*. Mineralogical Association of Canada Short Course Series, **42**, 133-165.

Mücher, H.J., De Ploey, J. and Savat, J. (1981) Response of loess materials to simulated translocation by water: micromorphological observations. *Earth Surface Processes and Landforms*, **6**, 331-336.

Muhs, D.R. (2007) Loess deposits, origins and properties. In: Elias, S. (ed), *Encyclopedia of Quaternary Science*, Publication of an Organisation Other than the US Geological Survey, USGS, p. 1405-1418, doi:10.1016/B0-44-452747-8/00158-7.

Murphy, K. (1987) *Eolian origin of Upper Palaeozoic red siltstones at Mexican Hat and Dark Canyon, south-eastern Utah*. Unpublished M.S. Thesis, University of Nebraska Lincoln, Nebraska, 128pp.

Nesbitt H.W. and Young, G.M. (1982) Early Proterozoic climates and plate motions inferred from major element chemistry of lutites. *Nature*, **229**, 715–717.

Nettleton, W.D. and Chadwick, O.A. (1996) Late Quaternary, re-deposited loess-soil developmental sequences, South Yemen. *Geoderma*, **70**, 21-36.

Packham, G. (1955) Volume-, weight-, and number-frequency analysis of sediments from thin-section data. *Journal of Geology*, **63**, 50-58.

Péron, S., Bourquin, S., Fluteau, F. and Guillocheau, F. (2005) Paleoenvironment reconstructions and climate simulations of the Early Triassic: impact of the water and sediment supply on the preservation of fluvial systems. *Geodin. Acta*, **18**, 431–446.

Price, W. A. (1963) Physicochemical and environmental factors in clay dune genesis. *Journal of Sedimentary Petrology*, **33**, 766-778.

Pye, K. (1987) *Aeolian dust and dust deposits*. Academic Press, London, 334 pp.

Retallack, G.J., Veevers, J.V. and Morante, R. (1996) Global coal gap between Permian–Triassic extinction and Middle Triassic recovery of peat-forming plants, *Geological Society of America Bulletin*, **108**, 195–207.

Reynolds, R. C. (1980). Interstratified clay minerals. In: Brindley, G.,W. & Brown, G. (eds) *Crystal Structures of Clay Minerals and their X-Ray Identification*. Mineralogical Society Monograph No. **5**, 249-304.

Roscher, M., Stordal, F. and Svensen, H. (2011) The effect of global warming and global cooling on the distribution of the latest Permian climate zones. *Palaeogeography, Palaeoclimatology, Palaeoecology*, **309**, 186-200.

Royer, D.L., Berner, R.A., Montanez, I.P., Tabor N.J. and Beerling, D.J. (2004) CO₂ as the primary driver of Phanerozoic climate. *Geological Society of America Today*, **14**, 4–10.

Sahagian, D.L. and Proussevitch, A.A. (1998) 3D particle size distributions from 2D observations: stereology for natural applications. *Journal of Volcanology and Geothermal Research*, **84**, 173-196.

Soreghan, G.S. (1992) Preservation and paleoclimatic significance of eolian dust in the Ancestral Rocky Mountains province. *Geology*, **20**, 1111-1114.

Soreghan, G.S., Moses, A. M., Soreghan, M.J., Hamilton, M.A., Fanning, C.M. and Link, P.K. (2007) Palaeoclimatic inferences from upper Palaeozoic siltstone of the Earp Formation and equivalents, Arizona-New Mexico (USA). *Sedimentology*, **54**, 701-719.

Soreghan, M.J., Heavens, N., Soreghan, G.S., Link, P.K., and Hamilton, M.A. (2014) Abrupt and high-magnitude changes in atmospheric circulation recorded in the Permian Maroon Formation, tropical Pangea. *Geological Society of America Bulletin*, (in press), doi: 10.1130/B30840.1.

This article is protected by copyright. All rights reserved.

Soreghan, M.J., Soreghan, G.S. and Hamilton, M.A. (2002) Palaeowinds inferred from detrital-zircon geochronology of upper Paleozoic loessite, western equatorial Pangea. *Geology*, **30**, 695-698.

Spalletti, L.A., Arabe, A.E. and Morel, E.M. (2003) Geological factors and evolution of southwestern Gondwana Triassic plants. *Gondwana Research*, **6**, 119–134.

Stewart, S.A. (2007) Salt tectonics in the North Sea Basin: a structural style template for seismic interpreters. *In: Ries, A.C., Butler, R.W.H. & Graham, R.H. (eds) Deformation of the Continental Crust: The Legacy of Mike Coward.* The Geological Society, London, Special Publication, **272**, 361–396.

Tanner, L.H., Lucas, S.G. and Chapman, M.G. (2004) Assessing the record and causes of Late Triassic extinctions. *Earth Science Reviews*, **65**, 103–139.

Tramp, K.L., Soreghan, G.S. and Elmore, R.D. (2004) Paleoclimatic inferences from paleopedology and magnetism of the Permian Maroon Formation loessite, Colorado, USA. *Geological Society of America Bulletin*, **116**, 671-686.

Uličný, D. (2004) A drying-upward aeolian system of the Bohdašín Formation (Early Triassic), Sudetes of NE Czech Republic: record of seasonality and long-term palaeoclimate change. *Sedimentary Geology*, **167**, 17-39.

Vigorito, M. and Hurst, A. (2010) Regional sand injectite architecture as a record of pore pressure evolution and sand redistribution in the shallow crust: insights from the Panoche Giant Injection Complex, California. *Journal Geological Society of London*, **167**, 889-904.

Westphal, M., Bazhenov, M.L., Lauer, J.P., Pechersky, D.M. and Sibuet, J.C. (1986) Paleomagnetic implications on the evolution of the Tethys belt from the Atlantic Ocean to the Pamirs since the Triassic. *Tectonophysics*, **123**, 37-82.

Wilkins, A.D. (2016) *Characterisation of Triassic mudstones from the Central North Sea: sedimentological, mineralogical and pore system properties*. Unpublished PhD thesis, University Aberdeen, Aberdeen, 412pp.

Wilkins, A.D., Wilson, M.J., Morton, A.C., Hurst, A. and Archer, S.G. (2015) First recorded occurrence of detrital baddeleyite (ZrO_2) in sedimentary rock, (Smith Bank Formation, Triassic, Central North Sea). *Scottish Journal of Geology*, **51**, 185-189.

Wilson, M.J. (2013) *Rock-Forming Minerals Volume 3C - Sheet Silicates: Clay Minerals*, 2nd Edition, Geological Society of London, 736 pp.

Ziegler, K. (2006) Clay minerals of the Permian Rotliegend Group in the North Sea and adjacent areas. *Clay Minerals*, **41**, 355-393.

Ziegler, P.A. (1989) *Evolution of Laurussia: A study in Late Palaeozoic plate tectonics*. K. N. G. M. Genootschap (ed.). Kluwer Academic Publishers, Dordrecht, 102 pp.

FIGURE CAPTIONS

Fig. 1. (A) Approximate (enlarged) location of study area on a reconstruction of Triassic palaeogeography (after Blakey, 2005) including the main global wind circulation patterns. (B) Detailed location of study area including the positions of key wells 20/25-1 and 30/24-22.

Fig. 2. Summary lithostratigraphy of the Triassic onshore and offshore north-west Europe. Placing the Smith Bank Formation in the Induan and Olenekian has minimal biostratigraphic support (Brennand, 1975).

Fig. 3. Sedimentary logs of continuous core taken from wells (A) 20/25-1 (ca 45 ft/13.7 m) and (B) 30/24-22 (ca 49.4 ft/15.1 m), locations in Fig. 1. vfs = very-fine sand, fs = fine sand, ms = medium sand, cs = coarse sand, vcs = very-coarse sand, g = granules, fp = fine pebbles, mp = medium pebbles, cp = coarse pebbles, vcp = very coarse pebbles.

Fig. 4. Sedimentary facies from core in well 20/25-1. (A) Micaceous unstratified siltstone with a limited bleached reduction zone either side of the sub-horizontal discontinuity. Depth 5434.75' MD. (B) Grey/green-grey reduction areas in an unstratified siltstone without visible signs of organic matter or mineralisation associated with them. The reduced areas taper and branch vertically and horizontally, and are typically less than 10 mm across. Occasionally they coalesce to form larger reduction spots. The contact between the red-brown rock mass and the reduced areas is sharp. Sample SB06, depth 5437.6' MD. (C) A stratified siltstone with ripple-scale parallel-lamination and cross-lamination, centimetre-scale erosion surfaces, claystone rip-up clast lags and desiccation cracks. Depth 5456.25' MD.

Fig. 5. Sedimentary facies from core in well 30/24-22. (A) Laminated siltstone and very fine-grained sandstone within which sandstone laminae fine upward, are current-ripple laminated and have some rippled upper surfaces. Finer grain-sized units are darker and redder than the coarser units and there is an overall fining and darkening upward. An erosional surface down-cuts ca 5 mm and has a claystone clast lag. The field of view is 10 cm wide. Depth 9819.6' MD. (B) Shrinkage cracks filled with very fine-grained sandstone that are confined to individual beds of claystone and do not penetrate into the underlying very-fine sandstone. Scale bar is 1 cm. Depth 9822.5' MD. (C) A sedimentary dyke (>5 cm high) with both sharply discordant and partially disaggregated margins (yellow) with the host interlaminated siltstone (grey and red) and very fine-grained sandstone (predominantly white). Undisrupted sandstone contains ripple lamination and preserves rippled upper surfaces. Intraclasts of sandstone are present within the dyke, sometimes highly modified and fractured (area 'a'). A tiny (millimetre-aperture) pygmatic dyke 'b' is identified. The extrudite (sediment extrusion) is largely siltstone and most of the disrupted sandstone has stayed within the vent area. Sediment extrusion occurred onto a 3 to 5 mm thick sandstone unit (solid red line). Depth 9823.5' MD.

Fig. 6. Petrographic data from well 20/25-1. (A) Unstratified siltstone with a random grain fabric and abundant clay pellets. Framed area shows detail in (B). Plane-polarised light, sample SB06, depth 5448.8' MD. (B) Detail from (A) showing generally ellipsoidal clay pellets that are similar or slightly larger than sand grain-size quartz. Plane polarised light. (C) A large clay pellet surrounded by a matrix of randomly-oriented finer grains, mainly quartz and finer-grained clay pellets, in an unstratified siltstone. The sample has the highest sand content (14.2%) in well 20/25-1. Plane polarised light, sample SB08, depth 5421.7' MD. (D) Unstratified siltstone with three types of diagenetic dolomite: (i) euhedral rhombs; (ii) halite pseudomorphs; (iii) pore filling – all are zoned. Cross-polarised light, sample SB05, depth 5437.3' MD. Scale bars in images are 100 μm , except (B) where scale bar is 50 μm

Fig. 7. *Back-scattered electron (BSE)* micrographs of structureless siltstone showing (A) a randomly-oriented grain fabric defined by elongate minerals, typically sand-sized muscovite (sample SB05, scale bar = 200 μm) and (B) detail of the planar fabric formed by compacted platy clay mineral grains within the rounded clay pellet (dashed outline) and zoned dolomite pore-filling cement and rhombs in the groundmass (sample SB06, scale bar = 30.3 μm).

Fig. 8. Typical fine-grained lithologies from well 30/24-22. (A) Laminae in a coarse-grained siltstone where the bases of individual laminae are defined by concentrations of undifferentiated opaque heavy minerals. Plane polarised light. Scale bar is 100 μm . Sample EQ06, depth 9859.9' MD. (B) Very finely-laminated siltstone in which a 50 μm sub-rounded quartz grain defines the maximum thickness of the prominent quartz-rich, coarse-silt lamination. Plane polarised light. Scale bar is 100 μm . Sample EQ04, depth 9838.25' MD. (C) Claystone with two prominent (at this magnification) laminae defined by discontinuous single-grain layers of quartz silt. Crossed polars. Scale bar is 100 μm . Sample EQ06, depth 9859.9' MD.

Fig. 9. Lithological classification of Smith Bank Formation grain-size domains from samples from wells 20/25-1 and 30/24-22. Most plot in the siltstone field. Claystone only occurs in well 30/24-22. All data are derived from petrographic analysis.

Fig. 10. Grain-size histograms from selected grain-size domains in samples from well 20/25-1 and well 30/24-22. (A) Unstratified siltstone (loessite) from well 20/25-1 showing bi-modal grain-size distribution. Sample SB05, depth 5437.3' MD. (B) Stratified mudstone from well 20/25-1. Grain-size domain SB10b illustrating a definitive excess of fine material, i.e. negative skewness. Sample SB10, depth 5455.5' MD. (C) Stratified siltstone from well 20/25-1. Grain-size domain SB10a also showing a bi-modal distribution as seen in (A). Sample SB10, depth 5455.5' MD. (D) Stratified claystone from well 30/24-22. Grain-size domain EQ04a illustrating a definitive excess of fine material, predominantly less than 2 μm . Sample EQ04, depth 9822.4' MD. (E) In comparison to (D) the grain-size domain in EQ04a illustrates the increase in fine silt content (Φ 6 to Φ 8) that has been introduced within an otherwise stratified claystone by the presence of shrinkage cracks. Sample EQ04, depth 9838.25' MD from well 30/24-22. (F) Grain size domain EQ05a, a bioturbated siltstone from well 30/24-22 showing a bimodal grain-size distribution. Sample EQ05, depth 9845.5' MD. (G) Stratified siltstone from well 30/24-22. Grain-size domain EQ03b. Similar bi-modal distribution displayed as for the stratified siltstone in (C) from well 20/25-1. Sample EQ03, depth 9834.7' MD. (H) Histogram for grain-size domain EQ02b. A stratified siltstone from well 30/24-22 with significant proportion very fine sand. Sample EQ02, depth 9822.4' MD.

Fig. 11. Siltstone samples from (A) well 20/25-1 (sample SB06, depth 5448.8' MD) and (B) well 30/24-22 (sample EQ02, depth 9822.4' MD). Both samples are poor to very-poorly sorted but grain-size domain EQ02b is noticeably coarser. The majority of visually-resolvable grains are angular, the coarsest grains tending to have highest sphericity; note the more rounded character of the coarsest grain fraction in the central left field of view in (B). Samples (A) and (B) are highlighted by arrows in (C) and (D). Scale bars are 100 μm . (C) Cumulative frequency grain-size distribution data for (A) have a relatively tight grouping of curves that show that most samples and their grain-size domains have a moderately linear relationship between grain size and abundance. Exceptions are specific grain-size domains SB04b and SB10b from stratified samples SB04 and SB10, which contain significantly higher proportions of the $<10\ \mu\text{m}$ fraction. (D) A wide range of grain-size distributions are recorded from the samples, and their associated grain-size domains, from well 30/24-22 that confirm the visual observations in Fig. 3B. Four grain-size domains, EQ02a, EQ03a, EQ04a and EQ06, all have significantly larger $<2\ \mu\text{m}$ fractions than the others, and sample EQ02b has a significantly higher $>20\ \mu\text{m}$ fraction.

Fig. 12. Directional fabric data for the Smith Bank Formation displayed using equal area rose diagrams. All data are bidirectional. (A) Random fabric associated with unstratified siltstone (loessite) in well 20/25-1. (B) and (C), near horizontal planar fabric associated with stratified fine-grained samples from both wells. (D) Bi-modal fabric with a predominant near vertical orientation and a subordinate horizontal component associated with shrinkage cracks from well 30/24-22. (E) A significantly modified horizontal planar fabric – see (B) and (C) – that has been randomised by bioturbation, well 30/24-22.

Fig. 13. Bulk mineralogy. (A) Samples from well 20/25-1 and (B) samples from well 30/24-22 determined by X-ray random powder diffraction (XRPD).

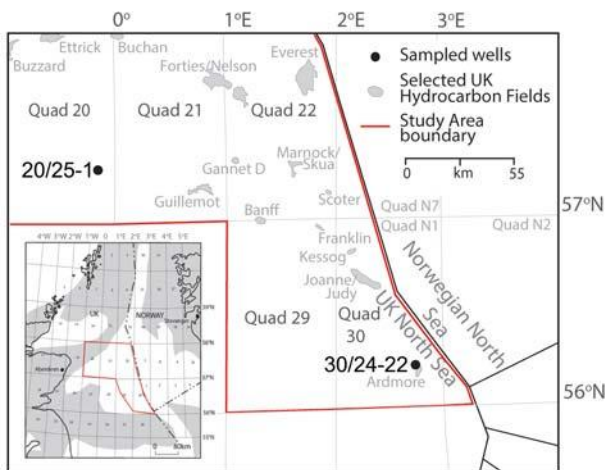
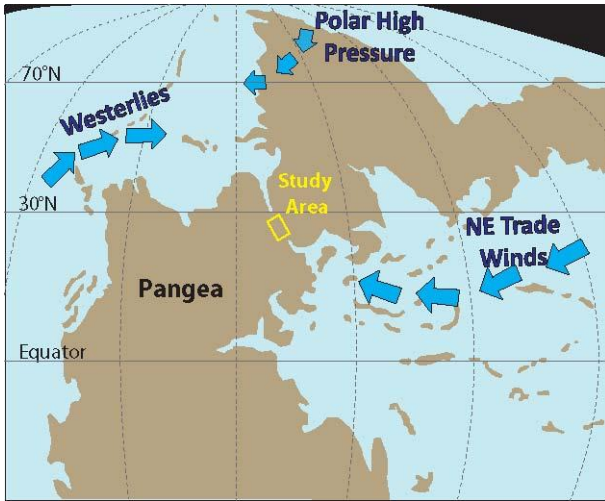
Fig. 14. X-ray diffraction (XRD) traces of oriented mounts of the $<2\ \mu\text{m}$ fraction: black trace air-dried, blue trace ethylene glycol-treated, red trace heated at 300°C , green trace 6N hydrochloric (HCl) acid treatment at 90°C for 30 min – (B) only. (A) Sample SB02, well 20/25-1 (CuK α radiation). Note the high spacing peak at $\sim 28\text{\AA}$ on a broad sloping background in the air-dried sample, the second-order basal reflection at about 16\AA after glycolation, the sharpened 10\AA peak after glycolation and the distinct kaolinite and chlorite peaks at 3.58 and 3.54\AA , respectively. (B) Sample SB01, well 20/25-1 (CoK α radiation). On the HCl-treated trace the high-spacing tosudite peak at $ca\ 28\text{\AA}$ is still present as well as the second order peak at $ca\ 14.5\text{\AA}$. Resistance to the acid treatment indicates that the mixed-layer chlorite-smectite is aluminous and hence is tosudite rather than corrensite. (C) Sample EQ01, well 30/24-22 (CuK α

radiation) with an illite-chlorite-illite/smectite (I/S) assemblage. The sharpening and intensification of the 10Å illite peak following glycolation and heating at 300°C, respectively are responses indicative of smectite mixed layering.

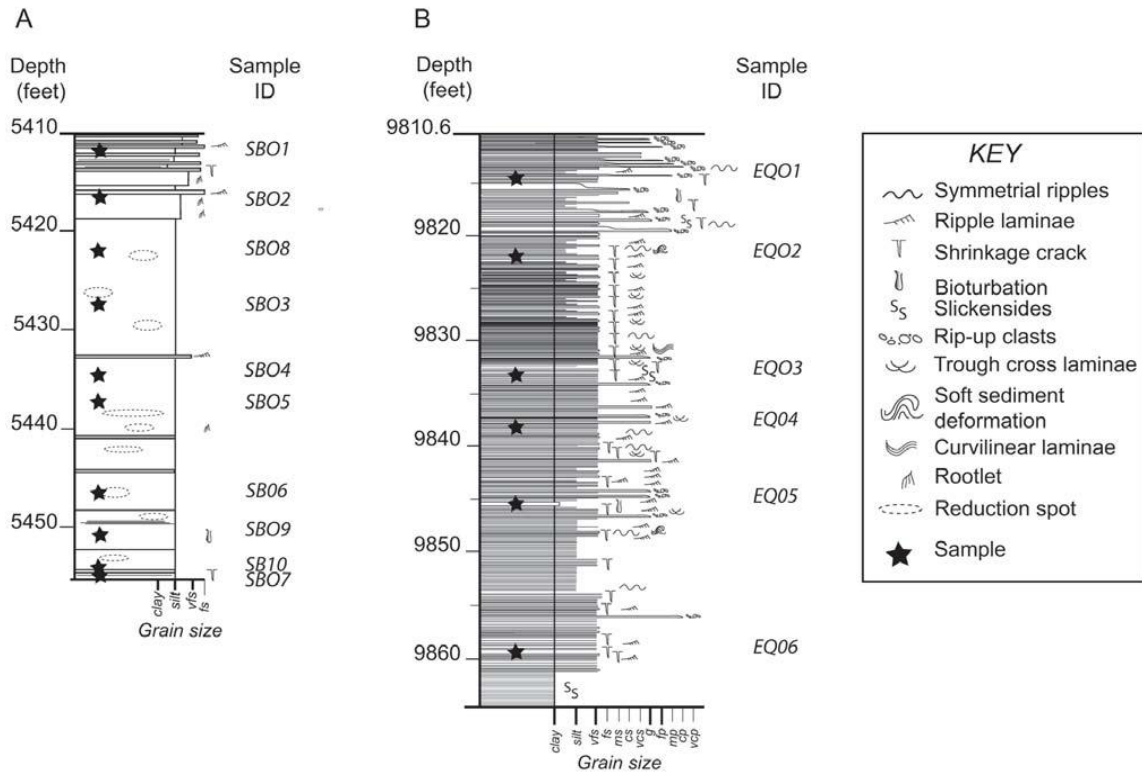
Fig. 15. Petrographic, compositional and grain fabric data from loessite outcrops. (A) Siltstone from the Halgaito Formation (Permian) by Mexican Hat, Utah. Sample MH02 illustrates the angular character of the quartz grains, particularly the triangular grain with three perfectly angular apices towards left centre of the figure. Scale bar in the image is 100 µm. (B) Siltstone from the Halgaito Formation (Permian). Sample MH01 has a random grain fabric and abundant silt-sized clay pellets. Scale bar in the image is 100 µm. (C) Lithological classification of the loessite samples. All plot within the siltstone field. MH – Mexican Hat, Halgaito Formation (Permian). PC – Parleys Canyon, Mahogany Member of the Ankareh Formation (Permian). (D) Directional fabric analysis shows that the Parleys Canyon sample has a random-oriented grain fabric, while the Mexican Hat sample MH01 has an approximate random distribution.

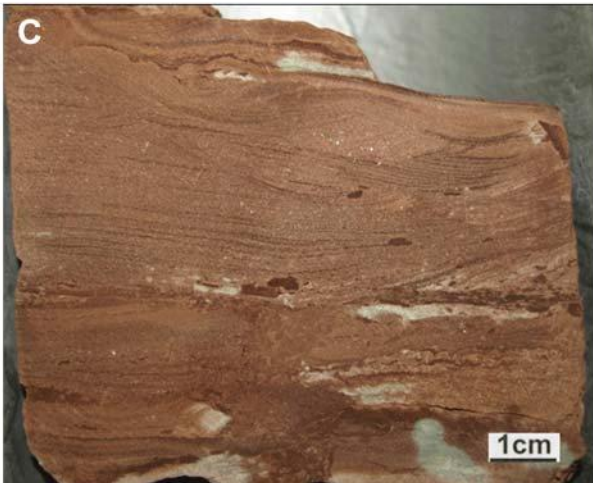
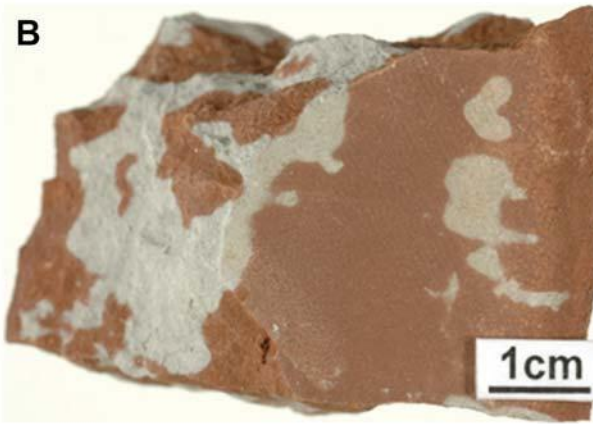
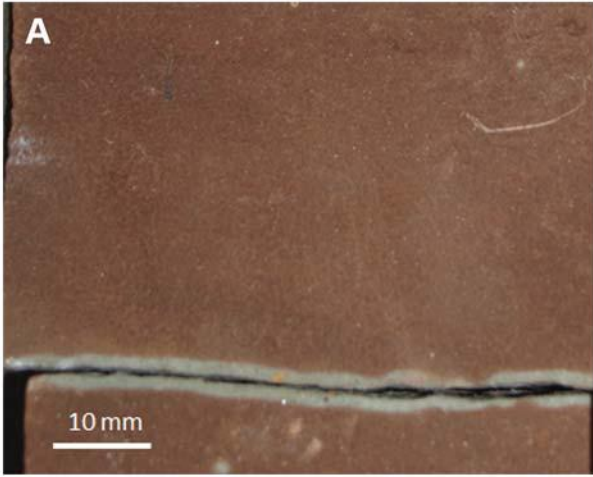
Fig. 16. Comparison of the cumulative grain-size distributions from unstratified siltstone from the Smith Bank Formation in well 20/25-1 and the ancient loessites in Fig. 15: MH – Mexican Hat, Halgaito Formation (Permian). PC – Parleys Canyon, Mahogany Member of the Ankareh Formation (Permian). All curves occur within the same relatively tight grouping that have a moderately linear relationship between grain size and abundance.

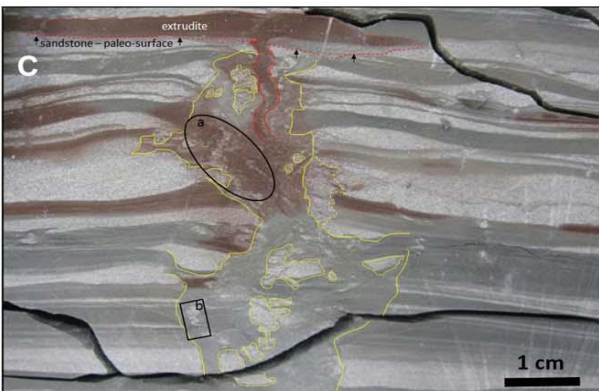
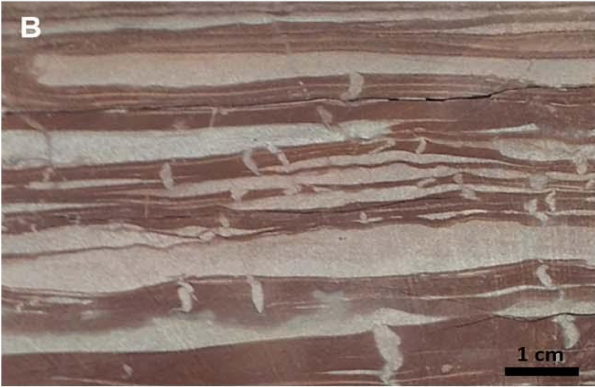
Fig. 17. (A) Palaeogeographic reconstruction of the lacustrine area (blue) in the North Permian Basin during the Early Triassic (Induan–Olenekian) modified from Goldsmith *et al.* (2003). The dashed line a northern shoreline defined by Bourquin *et al.* (2010). Locations of the study wells 20/25-1 and 30/24-22 are shown from which core was studied. (B) Revised palaeogeography of the lacustrine area based on data from this study. Loessite identified in well 20/25-1 implies that lacustrine conditions were absent at this location. In the absence of adjacent well data the distance for the lacustrine shore is estimated using data from the present-day Lake Erye. In the south (the pale blue area around 30/24-22) there is abundant evidence of persistent lacustrine conditions and the margin is expanded accordingly.

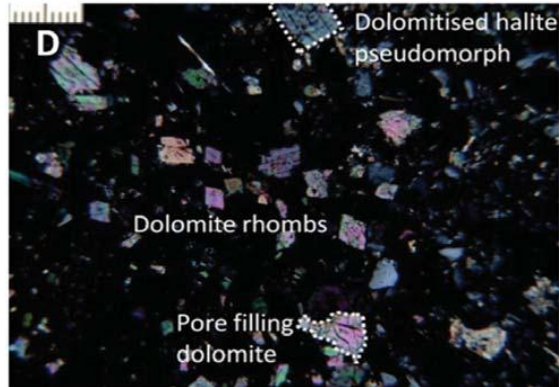
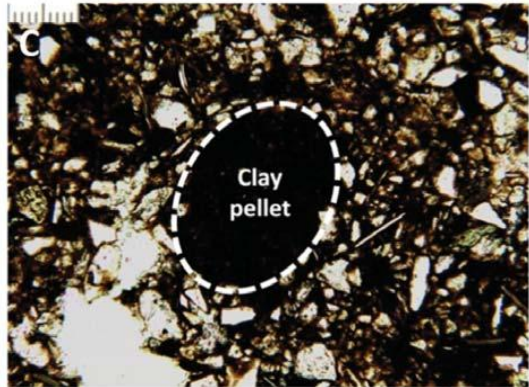
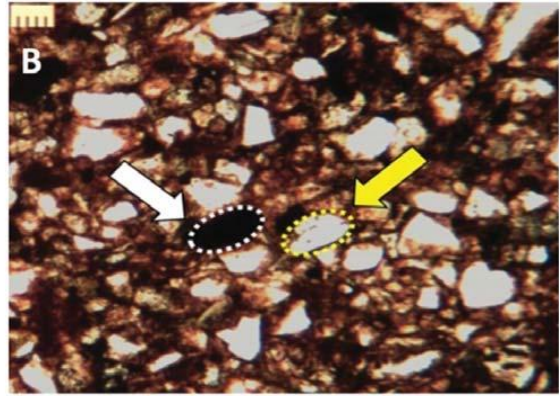
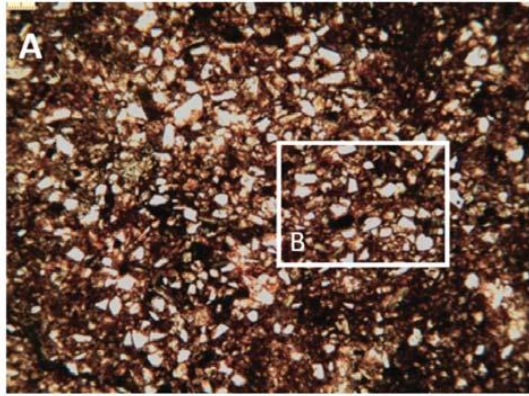


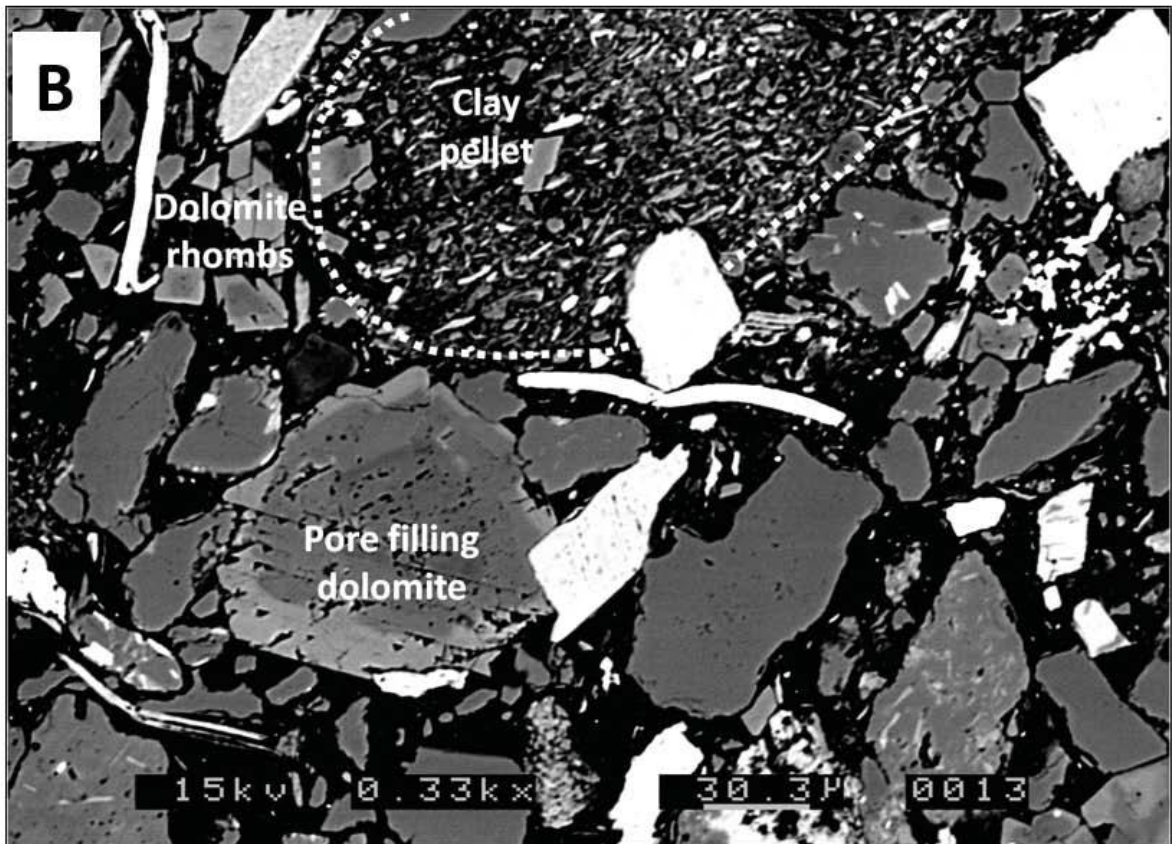
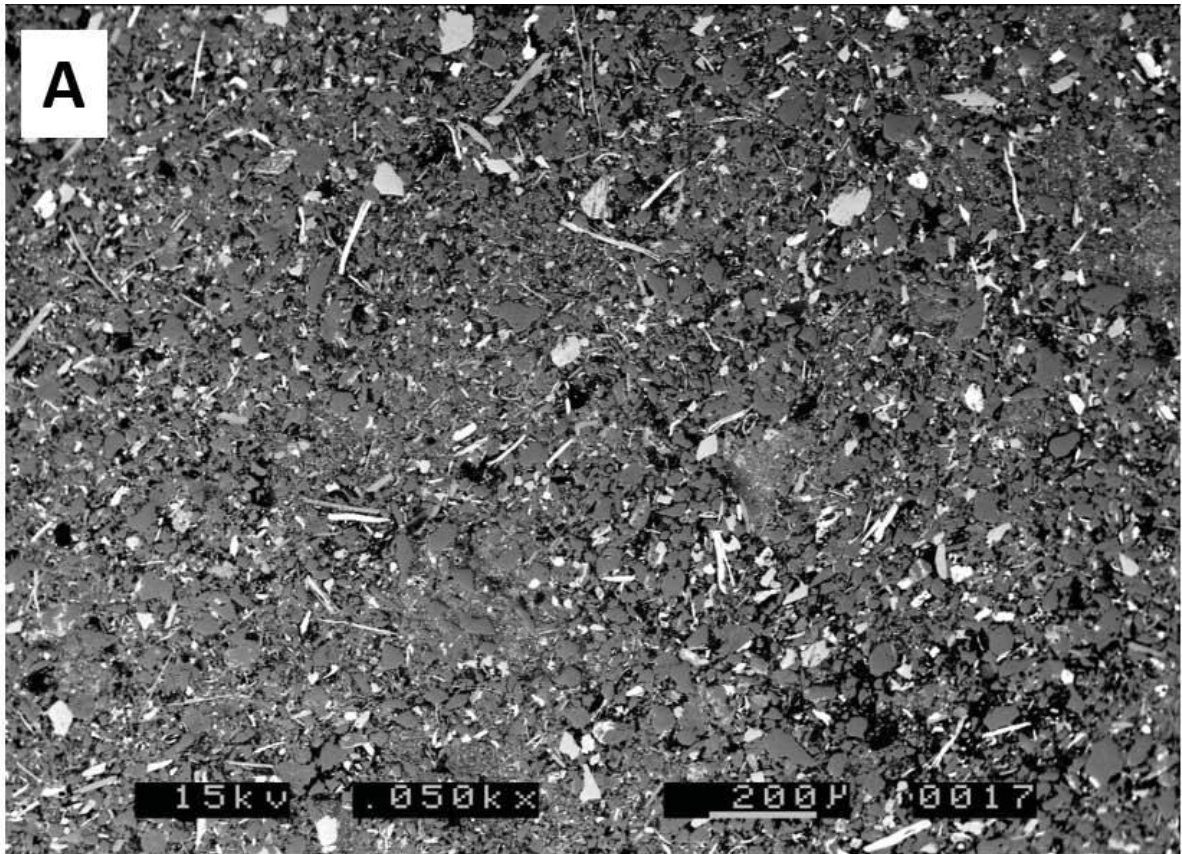
Series	Stage	Germany (Paul et al, 2009)	Onshore UK (Warrington et al, 1980)	Southern North Sea (Johnson et al, 1994)	Central North Sea (Goldsmith et al, 1995)	Northern North Sea (Steel & Ryseth, 1993)	
Upper	Rhaetian	Keuper	Penarth Group	Penarth Group	Skagerrak Formation	Joshua Mudstone Mbr	
	Norian		Mercia Mudstone Group	Hainsborough Group		Triton Formation	Josephine Sandstone Mbr
	Carnian					Dudgeon Formation	Jonathan Mudstone Mbr
Middle	Ladinian	Muschelkalk	Sherwood Sandstone Group	Dowsing Formation	Heron Group	Joanne Sandstone Mbr	
	Anisian					Julius Mudstone Mbr	
Lower	Olenekian	Buntsandstein	Bacton Group	Smith Bank Formation	Bunter Sandstone	Lomvi Formation	
	Induan					Teist Formation	

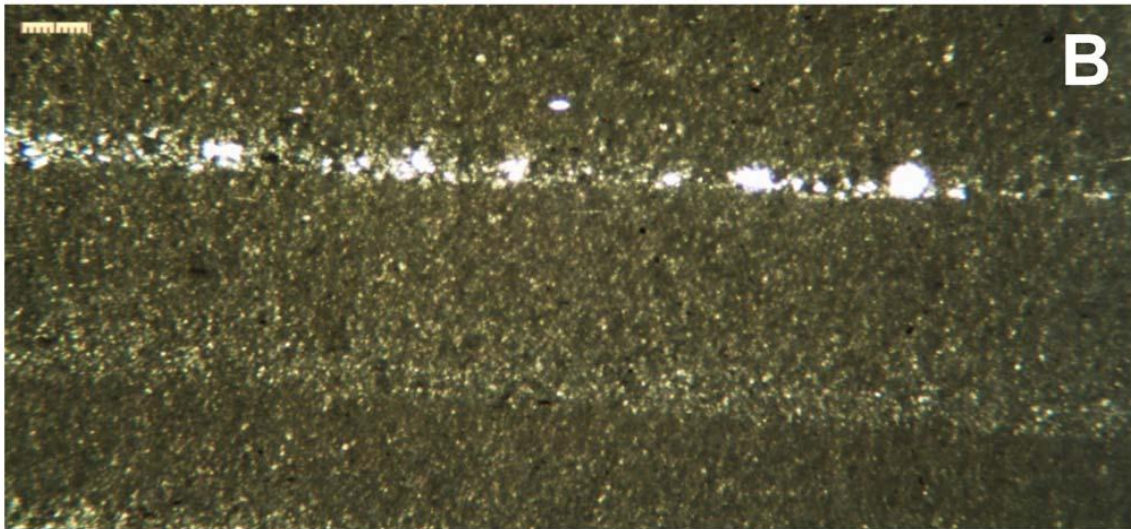
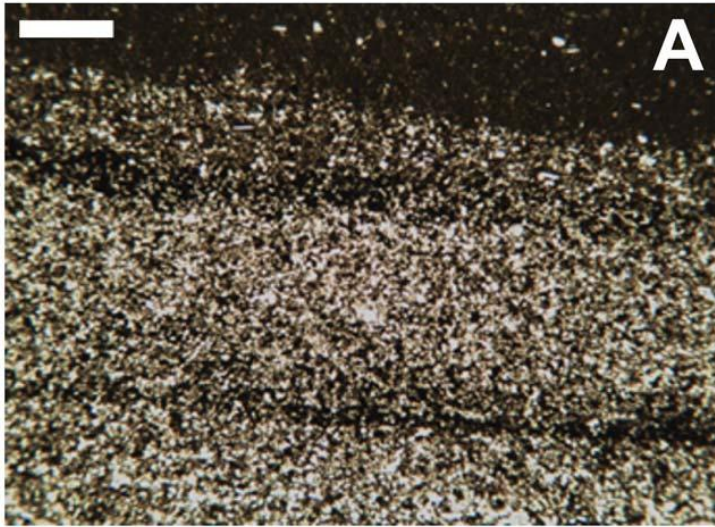


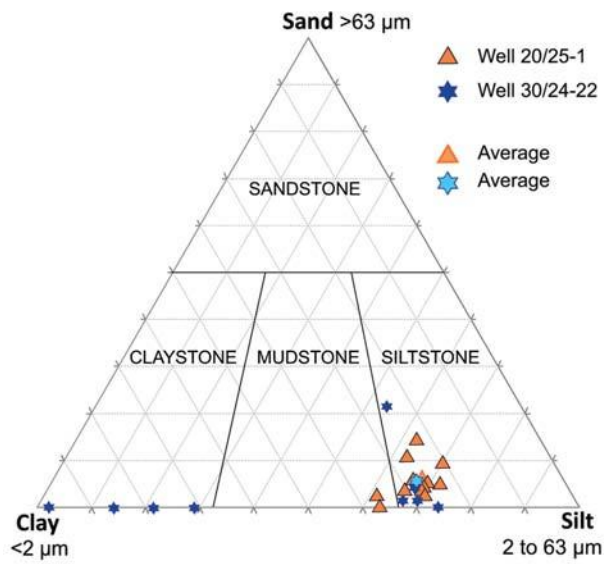
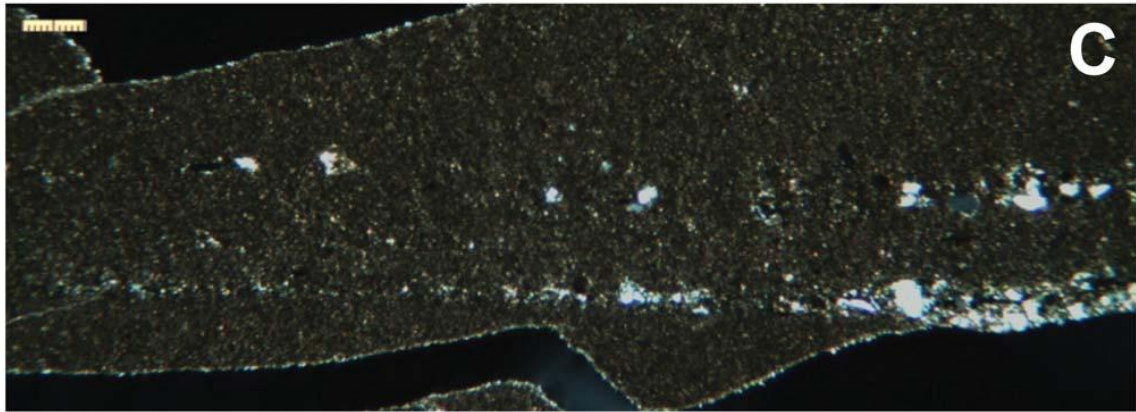


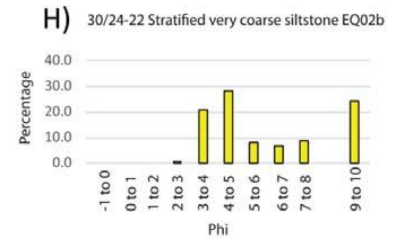
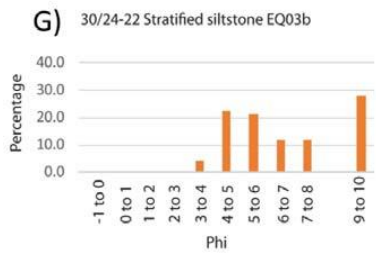
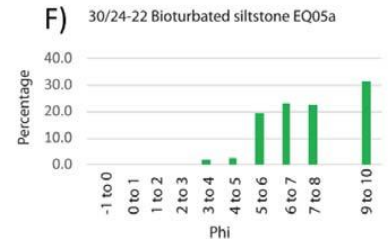
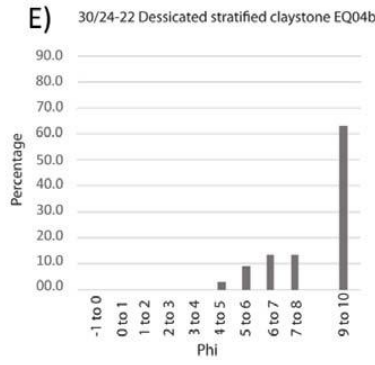
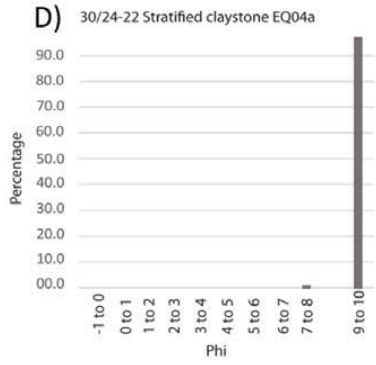
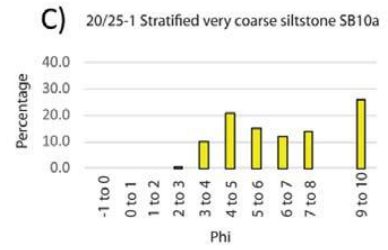
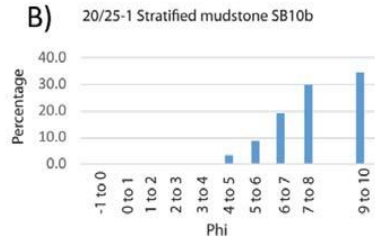
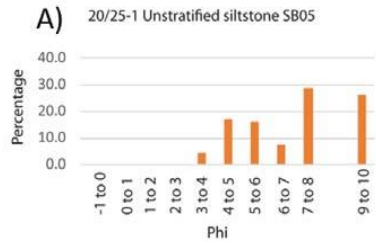


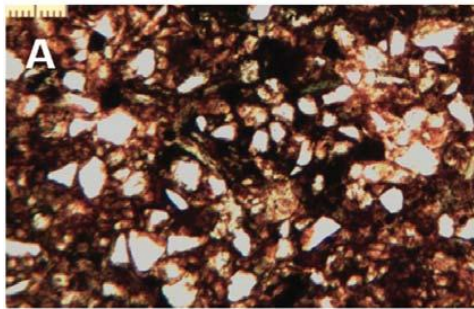




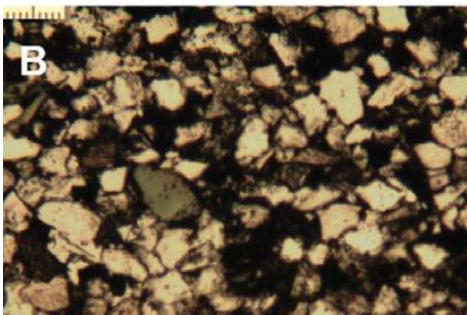
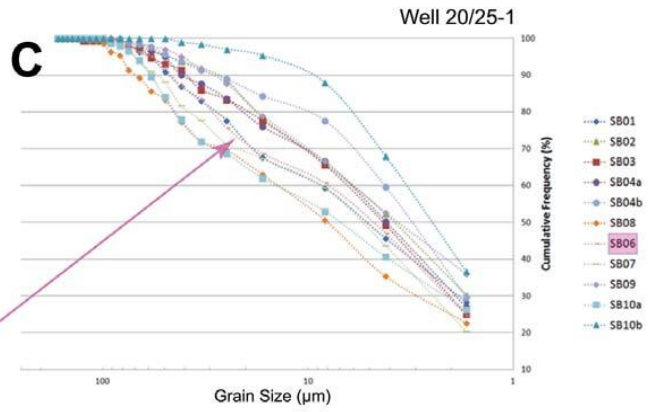




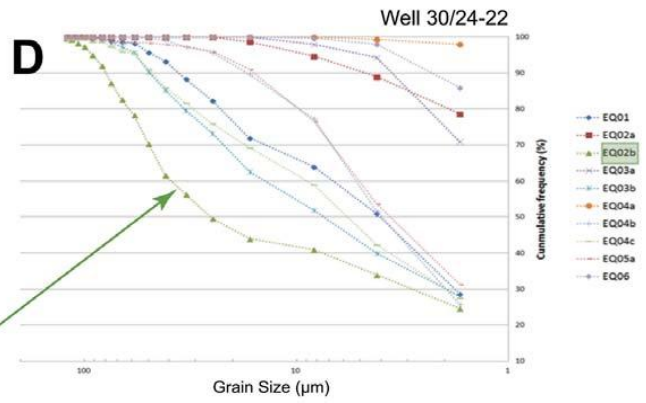


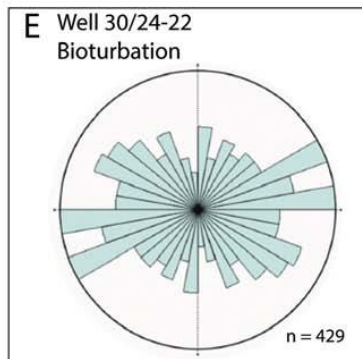
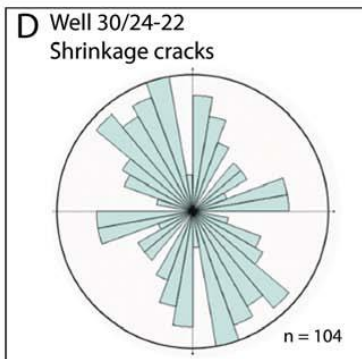
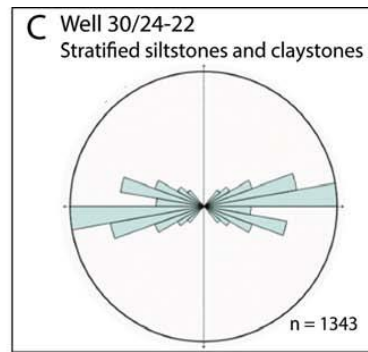
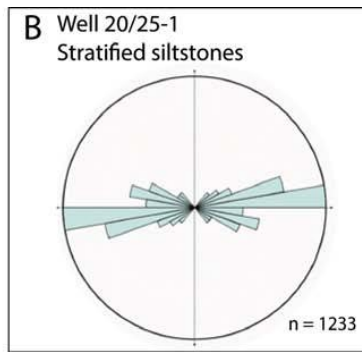
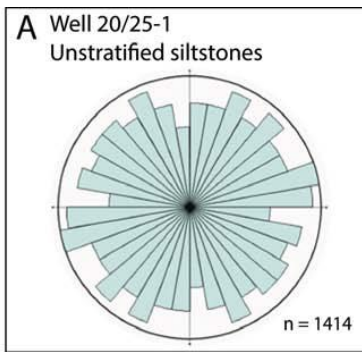


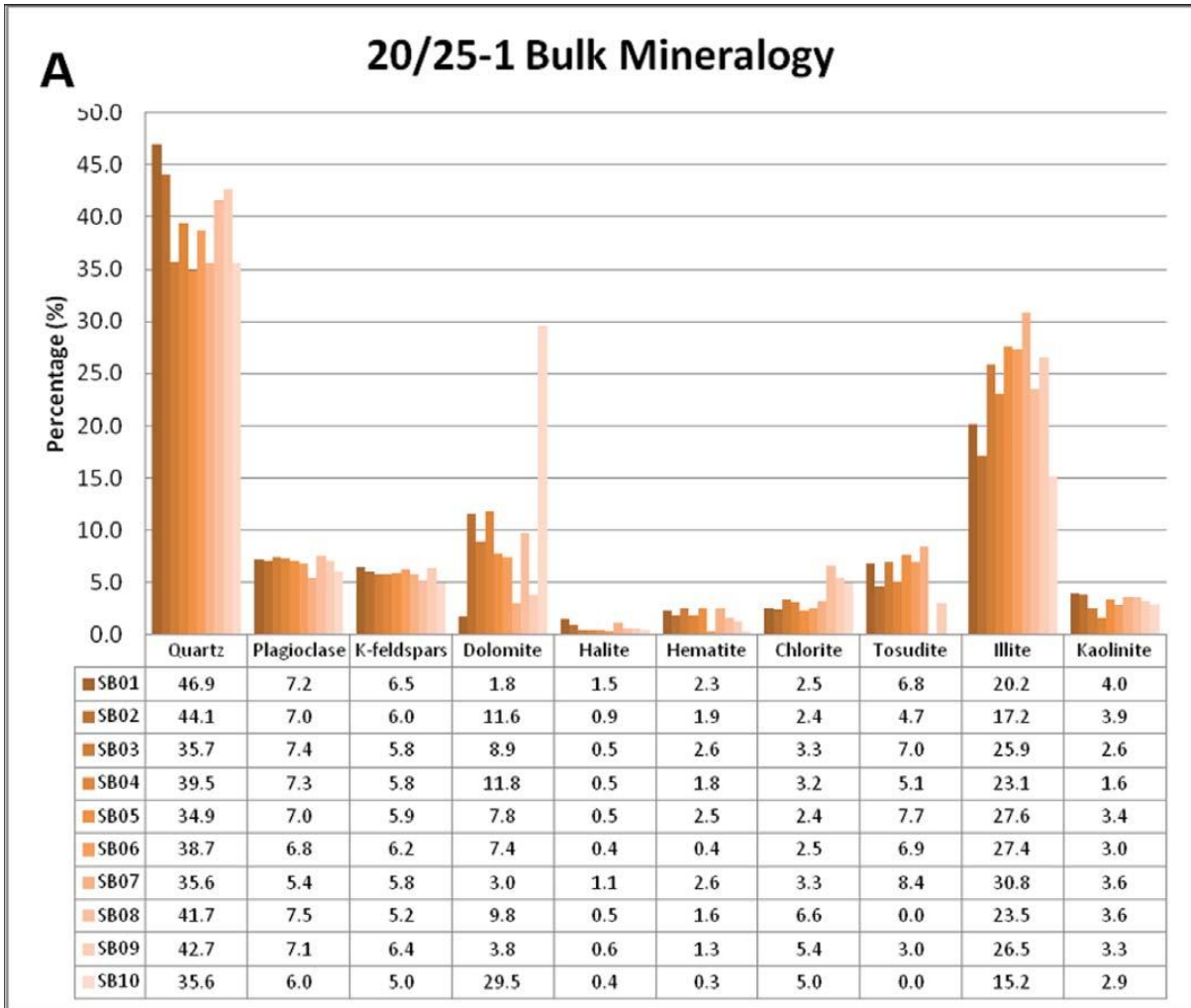
SB06 20/25-1 5448.8ft

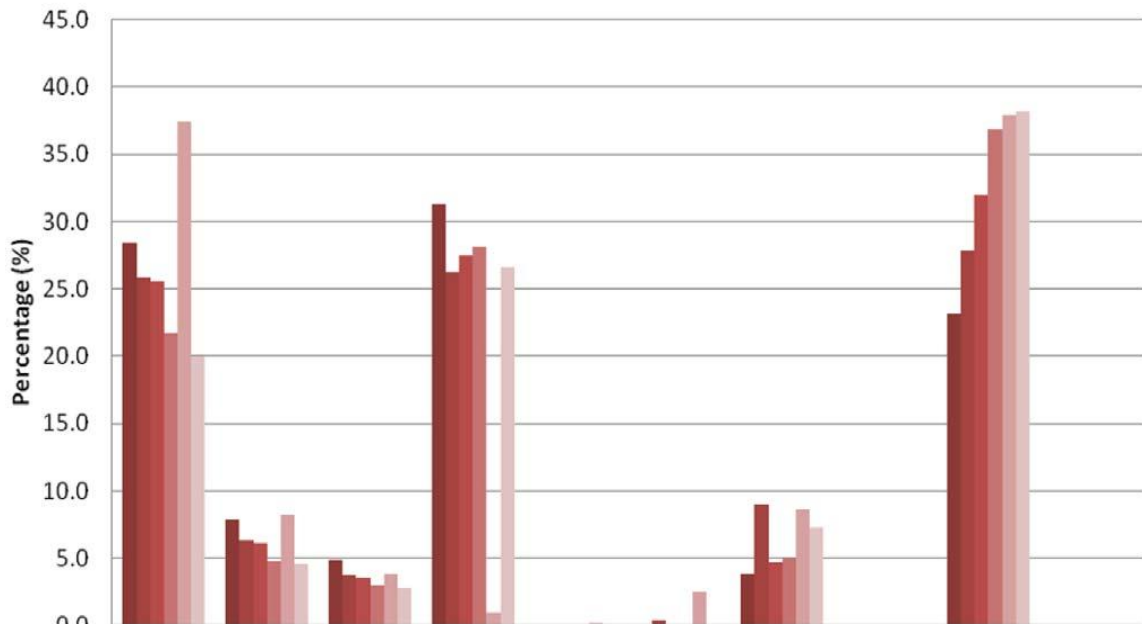


EQ02b 30/24-22 9822.4ft







B**30/24-22 Bulk mineralogy**

	Quartz	Plagioclase	K-feldspars	Dolomite	Halite	Hematite	Chlorite	Tosudite	Illite	Kaolinite
EQ01	28.4	7.9	4.9	31.3	0.1	0.0	3.8	0.0	23.1	0.0
EQ02	25.9	6.3	3.7	26.2	0.1	0.4	9.0	0.0	27.8	0.0
EQ03	25.5	6.1	3.6	27.5	0.1	0.0	4.7	0.0	32.0	0.0
EQ04	21.7	4.8	2.9	28.1	0.1	0.0	4.9	0.0	36.8	0.0
EQ05	37.4	8.3	3.9	0.9	0.1	2.4	8.6	0.0	37.9	0.0
EQ06	20.0	4.6	2.8	26.6	0.0	0.0	7.2	0.0	38.2	0.0

